

Lanfang Xie and Hongyi Chen contributed equally to this work.

Key Points:

- Northwest Africa (NWA) 12279 is a unique lunar meteorite that is both unbrecciated and pristine
- The magmatic melt inclusion in Mg-spinel represents the mixed composition between lunar mantle melt and anorthositic crust
- The formation of Mg-spinel in NWA 12279 results from the interaction between the mantle material and the anorthositic crust of the Moon

Correspondence to:

H. Chen,
Chy@glut.edu.cn

Citation:

Chen, H., Xie, L., Shu, Q., & Miao, B. (2023). Northwest Africa 12279: Evidence for the interaction between early lunar mantle melt and anorthositic crust. *Journal of Geophysical Research: Planets*, 128, e2023JE007844. <https://doi.org/10.1029/2023JE007844>

Received 1 APR 2023

Accepted 12 SEP 2023

Author Contributions:

Conceptualization: Hongyi Chen, Bingkui Miao

Data curation: Lanfang Xie, Qiao Shu

Formal analysis: Hongyi Chen, Lanfang Xie, Qiao Shu

Funding acquisition: Hongyi Chen

Investigation: Hongyi Chen, Lanfang Xie



Methodology: Hongyi Chen, Lanfang Xie

Resources: Hongyi Chen

Writing – original draft: Hongyi Chen, Lanfang Xie

Writing – review & editing: Hongyi Chen, Lanfang Xie, Bingkui Miao

Northwest Africa 12279: Evidence for the Interaction Between Early Lunar Mantle Melt and Anorthositic Crust

Hongyi Chen¹ , Lanfang Xie¹, Qiao Shu², and Bingkui Miao¹ 

¹Institution of Meteorites and Planetary Materials Research, Key Laboratory of Planetary Geological Evolution of Guangxi Provincial Universities, College of Earth Sciences, Guilin University of Technology, Guilin, China, ²Institute of Geochemistry, Chinese Academy of Sciences, Guiyang, China

Abstract The Mg-spinel-bearing rocks are an essential component of the lunar crust. They are widely distributed on the Moon's near and far sides. The study of petrogenesis provides a rare opportunity to understand the early lunar crust-mantle interaction. Northwest Africa 12279 is a unique Mg-spinel-bearing troctolitic anorthositic lunar meteorite that is unbrecciated and pristine. The modal content of the spinel-bearing troctolitic component is ~95%. Five hundred sixty spinels larger than 100 μm are investigated in this paper, and 38 of them are found to contain magma melt inclusions. These magma melt inclusions represent the mixed composition between mantle melt and crust material during the crystallization of a spinel. They generally show an immiscible liquid phase separation, which can be divided into a magnesium-rich and silica-rich phase. The former is similar in chemical composition to the lunar mantle's peridotite or plutonic ultramafic Mg-suite. The mantle melt reacts successively with Ferroan Anorthosites in the crust to crystallize Mg-spinel, plagioclase, olivine, pyroxene, and silica phases. The large grains of euhedral Mg-spinels with homogeneous chemical composition indicate they are the products of equilibrium crystallization, while plagioclase, olivine, pyroxene, and silica phase are the products of differentiated crystallization of mixed magma. This reaction may represent a typical process of lunar Mg-suite. This work is the first to find petrological evidence that the melt from the lunar mantle intrudes into the crust and then undergoes a liquid phase immiscible separation to form the Mg-spinel-bearing troctolitic anorthositic.

Plain Language Summary Northwest Africa 12279 (weight 1,830 g) is the only known pristine and unbrecciated lunar spinel-bearing troctolitic anorthositic, including lunar meteorites and returned samples. These pristine samples are indispensable for understanding Moon's history and chemical evolution. The spinel-bearing rocks are an essential component of the lunar crust. They are widely distributed on the Moon's near and far sides. The study of petrogenesis provides a rare opportunity to understand the early lunar crust-mantle interaction. Five hundred sixty spinels larger than 100 μm are investigated in three polished thin sections, and 38 contained magma melt inclusions. These magmatic inclusions represent the mixed composition between early mantle melt and crust material during the crystallization of a spinel. This work is the first to find evidence that the melt from the lunar mantle intrudes into the crust. The magnesium-rich melt from the mantle assimilates with ferroan anorthositic (an igneous rock is composed of >90 vol.% plagioclase rich in calcium with minor iron-rich pyroxene and olivine) from the early crust to form an Mg-spinel-bearing hypabyssal igneous rock.

1. Introduction

The theory of the lunar crust formation has been determined by the samples collected from the nearside of the Moon. Based on the analysis of the returned samples, a Lunar Magma Ocean (LMO) model was proposed (Smith et al., 1970; Walker & Hays, 1977; Wood, 1972) and developed (Elardo et al., 2011; Warren, 1985). The LMO model suggests that olivine and orthopyroxene were produced and then sunk to form the mantle (Warren, 1985), while plagioclase floated to create a Ferroan Anorthosites (FANs) crust (Walker & Hays, 1977). The final residual of LMO dregs becomes enriched with potassium (K), rare earth elements (REEs), phosphorus (P), typically KREEP, and other incompatible elements (Elardo et al., 2011; Warren, 1985). Late crystalline ilmenite sinks into the mantle due to its high density. The density difference (ilmenite have a density of 3.7–3.8 g/cm^3 , compared to the underlying olivine + pyroxene mantle density of ~3.3 g/cm^3) causes the overturn of the lunar mantle (Elkins-Tanton et al., 2002). The overturned mantle material was decompressed and then melted to form the parent magma of the Mg-suite (e.g., Borg et al., 2020; Gross et al., 2020; Prissel & Gross, 2020; Shearer et al., 2015).

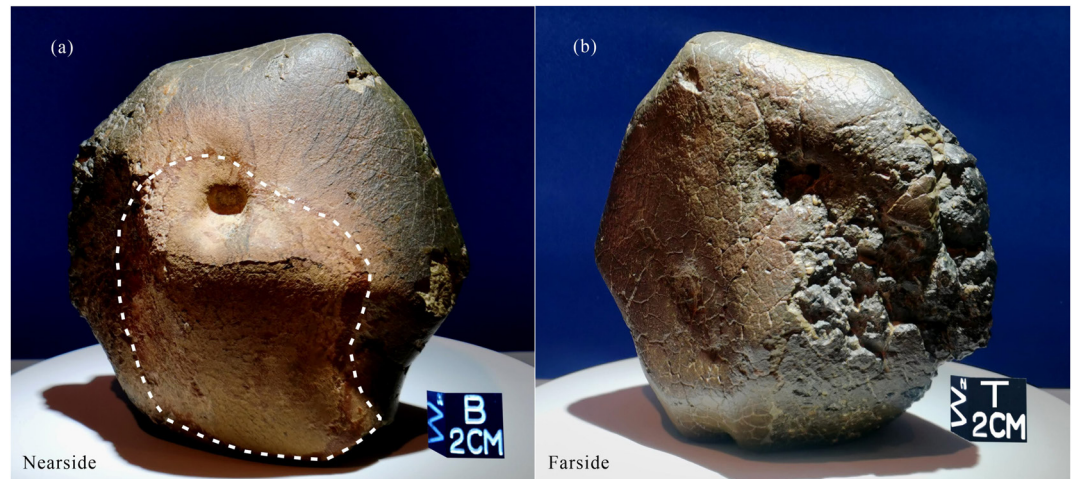


Figure 1. Appearance characteristics of lunar meteorite NWA12279. (a) Fusion crust and radial molten lines. The white dotted line shows the region buried under the sand when the sample was discovered. It was also at the forefront of the atmospheric path, judging from the direction of the molten lines. (b) Shrinkage fissures and impact melt on the surface. It shows the far side of the flight direction.

Prissel and Gross (2020) modeled partial melting of the lower mantle during overturn to produce Mg-suite primary melts. These melts could then crystallize to form troctolites and norites or react with the lunar crust to form Mg-spinel-bearing rocks. Similarly, Prissel and Gross (2020) suggest that the KREEP signature of some Mg-suite Apollo samples is acquired through magma mixing or assimilation of KREEP. As a potential contaminant during the emplacement of primary Mg-suite, KREEP melts into the crust, then explains the presence of both KREEP-bearing and KREEP-poor Mg-suite in the meteorite collection.

The Mg-suite igneous rock fragments and clasts are plutonic to hypabyssal in origin. There are a range of rock types, including ultramafics (e.g., dunites, pyroxenites, harzburgites, and peridotites), troctolites, pink spinel troctolites (PST), anorthositic troctolites, norites, and gabbro-norites (Shearer et al., 2015). Primitive olivine (high $Mg^{\#}$ = molar, $Mg/(Mg + Fe) \times 100$), spinel (high $Mg^{\#}$ and $Al^{\#}$ = molar, $Al/(Al + Cr + Ti) \times 100$), and calcic-plagioclase (high An = molar, $Ca/(Ca + Na + K) \times 100$) dominate the mineralogy of the spinel-bearing lithologies. These features also belong to Mg-suite rocks (Shearer et al., 2015). Therefore, there is no doubt that the spinel-bearing lithologies belong to the Mg-suite. PST and pink spinel anorthosite (PSA) are two lunar lithologies known to contain Mg-spinel. Unfortunately, less than 1 mm PST fragments were found in the returned lunar samples and meteorites (Gross & Treiman, 2011; Marvin et al., 1989; Prinz et al., 1973). It is uncertain whether these fragments represent the whole parent rock. PSA rich in spinel and lacking mafic minerals, were detected by the Moon Mineralogy Mapper (M^3) of the Chandrayaan-1 spacecraft (Pieters et al., 2011). They are widely distributed on the tops of the central peaks and along the inner basin ring of the large impact craters. They are found on the Moon's near and far side (Pieters et al., 2011; Sun et al., 2017). The PSA characteristics suggest that they originated in the lower crust or crust-mantle boundary and were exposed to the lunar surface through impact sputtering (Gross & Treiman, 2011; Prissel et al., 2012, 2014). However, no sample that fully meets the characteristics of a PSA interpreted by remote sensing has been found. Therefore, NWA 12279 offers a rare opportunity to study the spinel formation on the Moon.

Any lunar rock fragment that escaped grinding, melting, mixing, and retained an endogenetic igneous composition and texture, is classified as “pristine” (Warren, 1993). Studying pristine samples (Shearer et al., 2015; Warren, 1993) to understand the Moon's history and chemical evolution is essential. However, such samples are scarce due to the strong impact and space weathering (Shearer et al., 2015). The lunar meteorite NWA 12279 (weight 1,830 g) is an unbrecciated and pristine Mg-spinel-bearing rock (Figure 1). According to Warren (1993)'s criteria for the primitiveness of the highland rocks, we are convinced that NWA 12279 is at a confidence level of 9 (highest degree). This value indicates that it represents nearly chemically unaltered Mg-suite lithology (the primary evidence is found in the discussion section of this paper). The magma melt inclusions in the Mg-spinels may represent the composition of a mixture between mantle melt and anorthositic crust. The coarse-grained plagioclases have similar characteristics to the FANs found in the lunar highland crust. NWA 12279 lunar meteorite

Table 1
The Mineral Content (vol. %) in Three Polished Sections of Northwest Africa 12279

Numbers	Size (mm)	Shape	Plagioclase	Olivine	Pyroxene	Spinel	Silica phase	Glass	Other minerals	Numbers of spinel > 100 μm	Distribution density (spinel/ mm^2)
NWA 12279, 1	23 × (2–7)	Crescent	81.9	11.2	4.11	1.45	1.06	0.21	0.07	56	0.61
NWA 12279, 2	25 × 18	Rectangle	81.8	12.5	3.08	1.24	0.98	0.3	<0.01	248	0.55
NWA 12279, 3	26 × 21	Rectangle	81.7	13	3.19	0.84	0.9	0.37	<0.01	256	0.47
Average	N. A.	N. A.	81.8	12.2	3.46	1.18	0.98	0.29	<0.01	N. A.	0.59

Note. Other minerals include taenite, kamacite, ilmenite, and terrestrial secondary calcite. N. A. means not applicable. Glass refers to the impact glass, excluding maskelynite.

records the petrological and geochemical evidence that the mantle melt intrudes into the ancient crust to form the Mg-spinel-bearing troctolitic anorthosite.

2. Sample and Analytical Methods

NWA 12279 is a pristine Lunar meteorite. This study uses three polished sections from the unbrecciated sample (Table 1). 100 mg of sub-samples are collected from some fragments (particle size ~ 1 mm) in five different areas from the rim to the core of the unbrecciated thin section. These fragments can represent the average composition of the whole rock except for impact melt. The fragments were ground to less than 20 μm with an agate mortar. Therein, samples of 30 mg are analyzed by the New Microprobe Fused Bead (NMFB, Xie et al., 2023) method for major bulk elements, and samples of 70 mg are measured using Inductively Coupled Plasma Mass Spectrometry (ICP-MS) for bulk trace elements.

2.1. Petrography and Principal Element Analysis

Petrographic observations were performed using a Zeiss Σ IGMA Field Emission scanning electron microscope (SEM) at the Guilin University of Technology. Backscattered electron (BSE) images of carbon-coated polished thin sections were obtained using SEM. An electron beam with an accelerating voltage of 15 kV and a 20 nA current is used. The X-ray mapping and the modes of the minerals (vol.%) (Table 1) are obtained using a TESCAN Integrated Mineral Analyzer (TIMA) system at the State Key Laboratory of Continental Dynamics, Northwest University, Xi'an, China. TESCAN Integrated Mineral Analyzer is an SEM and energy disperse spectroscopy based automated mineralogy system comprising a TESCAN MIRA-3 SEM equipped with four EDS detectors and mineral data processing software. TESCAN Integrated Mineral Analyzer automatically identifies and quantifies minerals based on the BSE signal intensity and characteristic X-rays spectrum. During analysis, the dot mapping analysis mode was chosen with X-ray counts set to 10,000, pixel spacing of BSE set to 1.5 μm , and dot spacing of EDS set to 4.5 μm . The measurements were conducted at an acceleration voltage of 25 kV, a current of 9 nA, and a working distance of 15 mm. The beam current and BSE signals are calibrated by platinum Faraday cup and EDS signals by Mn standard (Hrstka et al., 2018).

The mineral composition was measured using a JEOL-JXA 8230 electron probe micro-analyzer (EPMA) at the Guilin University of Technology with an accelerating voltage of 15 kV. The plagioclase was analyzed using a current of 10 nA and a 5 μm diameter electron beam. Spinel, melt inclusion, olivine, and pyroxene were analyzed using a focused electron beam (<1 μm) and a current of 20 nA. The measurement times for elemental peak and background are 20 and 10 s, respectively, for most elements, except for Na and K (10 and 5 s for peak and background measurements, respectively). Natural and synthetic crystals were used as standards for the analyses. The standard materials used for the calibration of measured elements and their limit of detection (ppm) were: Si (olivine, 130); Ti (rutile, 294); Al (albite, 88); Cr (Cr metal, 83); Fe (olivine, 154); Mn (MnO, 104); Mg (olivine, 130); Ca (wollastonite, 91); Na (albite, 97); K (phlogopite, 77); and Ni (Ni metal, 201). The same analytical conditions were used for the standard materials and all mineral phases. All data were reduced with the ZAF procedure. All the microprobe data are given in Table 2.

2.2. Bulk Compositions

Bulk compositions of major elements were measured using an NMFB at the Institute of Geochemistry, the Chinese Academy of Sciences for sample preparation, and the Guilin University of Technology for EPMA analysis. This method improves the MFB method commonly used for the Apollo samples (Brown, 1977). It solves the problems of volatilization of the low-boiling elements and the rapid crystallization of high-melting point minerals such as Mg-spinel and forsterite. The main procedures are referred to by Xie et al. (2023). The data are presented in Table 2.

2.3. Trace Elements

Whole-rock trace elements were determined using an Agilent 7700 cx ICP-MS using the chemical dissolution method at the Guilin University of Technology. In situ trace element analysis of massive plagioclase

Table 2
Major Elements in the Minerals, Magma Melt Inclusions, and Whole Rock of Northwest Africa 12279

Minerals	Plagioclase		Spinel		Olivine			Pyroxene			Magma melt inclusions in Spinel			Whole rock
	Coarse-grained	Fine-grained	Core	Rim	Core	Rim	Pigeonite	Augite	Silica phase	Mg-rich	Si-rich	Spinel		
<i>n</i>	65	13	51	22	43	48	13	55	42	38	15	35		
Oxide														
SiO ₂	43.9 ± 0.85	44.0 ± 0.92	0.11 ± 0.08	0.30	38.5 ± 1.05	37.8 ± 1.31	50.1 ± 1.64	49.7 ± 1.21	97.6 ± 0.57	47.9 ± 1.50	62.1 ± 3.25	45.8 ± 0.34		
TiO ₂	0.04	0.02	0.10	0.21 ± 0.20	0.04	0.05	0.83 ± 0.47	1.04 ± 0.48	0.24 ± 0.08	0.35 ± 0.10	0.17 ± 0.08	0.18		
Al ₂ O ₃	35.8 ± 0.80	35.4 ± 0.83	64.8 ± 0.89	61.9 ± 3.20	0.11 ± 0.10	0.10	1.82 ± 0.82	2.55 ± 1.25	0.92 ± 0.33	12.2 ± 2.25	21.3 ± 2.10	27.3 ± 0.19		
Cr ₂ O ₃	0.01	0.02	4.42 ± 1.30	5.60 ± 2.79	0.15 ± 0.06	0.15 ± 0.06	0.21 ± 0.15	0.41 ± 0.17	0.02	0.26 ± 0.12	0.27 ± 0.21	0.09 ± 0.03		
FeO	0.33 ± 0.14	0.36 ± 0.16	7.42 ± 0.43	10.6 ± 1.78	18.3 ± 2.87	23.7 ± 4.87	22.6 ± 6.34	16.6 ± 4.92	0.28 ± 0.13	6.31 ± 1.65	1.84 ± 0.49	1.91 ± 0.12		
MnO	0.01	0.01	0.05 ± 0.02	0.10	0.23 ± 0.05	0.29 ± 0.08	0.39 ± 0.12	0.35 ± 0.10	0.01	0.14 ± 0.05	0.04 ± 0.03	0.07 ± 0.02		
MgO	0.23 ± 0.15	0.30 ± 0.10	22.7 ± 0.47	20.7 ± 1.28	42.2 ± 2.27	37.5 ± 3.76	15.5 ± 3.73	12.7 ± 2.42	0.03	17.5 ± 2.34	3.78 ± 1.37	7.76 ± 0.11		
CaO	19.3 ± 0.66	19.3 ± 0.52	0.03	0.25	0.34 ± 0.08	0.37 ± 0.11	8.40 ± 2.93	16.5 ± 2.42	0.39 ± 0.17	15.0 ± 2.92	9.11 ± 1.56	16.1 ± 0.16		
Na ₂ O	0.26 ± 0.08	0.53 ± 0.18	0.01	0.03	0.02	0.02	0.04 ± 0.03	0.06 ± 0.02	0.08 ± 0.05	0.10 ± 0.06	0.86 ± 0.34	0.47 ± 0.04		
K ₂ O	0.02 ± 0.01	0.01	0.01	0.01	0.02	0.02	0.03 ± 0.01	0.03	0.03 ± 0.02	0.04 ± 0.03	0.10	0.04 ± 0.01		
NiO	B. D.	B. D.	0.02	0.01	B. D.	0.01	0.04 ± 0.02	B. D.	B. D.	N. A.	N. A.	0.01		
P ₂ O ₅	0.01	B. D.	0.01	B. D.	0.01	0.02	0.01	0.02	0.01	0.02	0.02	0.01		
Total	99.9 ± 0.54	100 ± 0.51	99.8 ± 0.45	99.7 ± 0.44	99.8 ± 0.48	100 ± 0.57	100 ± 0.49	100 ± 0.47	99.7 ± 0.29	99.7 ± 0.38	99.5 ± 0.26	99.7 ± 0.26		
afu														
Si	2.04 ± 0.04	2.04 ± 0.03	B. D.	0.01 ± 0.03	0.98 ± 0.02	0.99 ± 0.01	1.92 ± 0.03	1.90 ± 0.03	1.97 ± 0.01	7.06 ± 0.46	8.08 ± 0.5	6.41 ± 0.03		
Ti	B. D.	B. D.	B. D.	B. D.	B. D.	B. D.	0.02 ± 0.01	0.03 ± 0.01	B. D.	0.04 ± 0.01	0.02 ± 0.01	0.02		
Al	1.95 ± 0.04	1.93 ± 0.05	1.91 ± 0.02	1.86 ± 0.14	B. D.	B. D.	0.08 ± 0.04	0.11 ± 0.05	0.02 ± 0.01	2.15 ± 0.49	3.31 ± 0.42	4.51 ± 0.03		
Cr	B. D.	B. D.	0.09 ± 0.03	0.11	B. D.	B. D.	0.01	0.01	B. D.	0.03 ± 0.01	0.03 ± 0.02	0.01		
Fe	0.01	0.01	0.15 ± 0.01	0.23 ± 0.04	0.39 ± 0.07	0.52 ± 0.12	0.73 ± 0.22	0.53 ± 0.17	B. D.	0.72 ± 0.25	0.26 ± 0.14	0.22 ± 0.01		
Mn	B. D.	B. D.	B. D.	B. D.	0.01	0.01	0.01	0.01	B. D.	0.02 ± 0.01	0.01	0.01		
Mg	0.02 ± 0.01	0.02 ± 0.01	0.84 ± 0.02	0.78 ± 0.04	1.60 ± 0.07	1.46 ± 0.12	0.88 ± 0.19	0.72 ± 0.13	B. D.	3.53 ± 1.02	1.03 ± 0.71	1.62 ± 0.02		
Ca	0.96 ± 0.03	0.96 ± 0.03	B. D.	0.01	0.01	0.01	0.34 ± 0.12	0.68 ± 0.09	0.01	2.24 ± 0.51	1.40 ± 0.47	0.42 ± 0.03		
Na	0.02 ± 0.01	0.05 ± 0.02	B. D.	B. D.	B. D.	B. D.	B. D.	B. D.	B. D.	0.04 ± 0.05	0.19 ± 0.09	0.01 ±		
K	B. D.	B. D.	B. D.	B. D.	B. D.	B. D.	B. D.	B. D.	B. D.	0.01 ± 0.01	0.02 ± 0.01	0.13 ± 0.01		
Ni	B. D.	B. D.	B. D.	B. D.	B. D.	B. D.	B. D.	B. D.	B. D.	N. A.	N. A.	N. A.		
P	B. D.	B. D.	B. D.	B. D.	B. D.	B. D.	B. D.	B. D.	B. D.	B. D.	B. D.	N. A.		
Total	5.00 ± 0.01	5.02 ± 0.01	3.00 ± 0.01	3.00 ± 0.01	3.00 ± 0.01	3.00 ± 0.01	4.01 ± 0.01	4.01 ± 0.01	2.01 ± 0.01	15.8 ± 0.53	14.33 ± 0.54	15.4 ± 0.03		

Table 2
Continued

Minerals	Plagioclase		Spinel		Olivine			Pyroxene			Magma melt inclusions in Spinel			Whole rock
	Coarse-grained	Fine-grained	Core	Rim	Core	Rim	Pigeonite	Augite	Silica phase	Mg-rich	Si-rich	Whole rock		
<i>n</i>	65	13	51	22	43	48	13	55	42	38	15	35		
Mg [#]	N. A.	N. A.	85.5 ± 0.81	77.6 ± 3.87	80.4 ± 3.35	73.8 ± 6.09	55.0 ± 12.8	58.0 ± 11.1	N. A.	82.4 ± 4.57	79.2 ± 3.11	87.9 ± 0.68		
Al [#]	N. A.	N. A.	95.6 ± 1.28	94.2 ± 2.96	N. A.	N. A.	91.3 ± 5.15	90.0 ± 2.82	N. A.	98.5 ± 0.92	99.0 ± 0.55	99.8 ± 0.07		
Ti [#]	N. A.	N. A.	0.16 ± 0.21	0.35 ± 0.33	N. A.	N. A.	23.8 ± 9.27	21.8 ± 9.53	N. A.	1.79 ± 0.92	0.55 ± 0.34	0.41		
Fe/Mn	N. A.	N. A.	N. A.	N. A.	79.1 ± 9.65	81.0 ± 7.71	57.0 ± 4.87	47.0 ± 5.59	N. A.	N. A.	N. A.	N. A.		
An/Fa/Fs	97.6 ± 0.79	95.2 ± 1.60	N. A.	N. A.	19.6 ± 3.35	26.3 ± 6.09	37.3 ± 11.3	27.5 ± 8.53	N. A.	N. A.	N. A.	N. A.		
Ab/Wo	2.35 ± 0.76	4.73 ± 1.58	N. A.	N. A.	N. A.	N. A.	17.6 ± 6.03	35.0 ± 4.85	N. A.	N. A.	N. A.	N. A.		

Note. *n* is the numbers of analysis points. afu means atoms per formula unit based on 8 oxygen atoms for plagioclase, 4 oxygen atoms for spinel and olivine, 6 oxygen atoms for pyroxene, 2 oxygen atoms for silicate phase or quartz, and 24 oxygen atoms for the magma melt inclusions in spinels and whole rock. B. D. means below detection; N. A. means not applicable. An and Ab are afu 100 × Ca/(Na + K + Ca) and 100 × Na/(Na + K + Ca) for plagioclase, respectively; Fa is afu 100 × Fe/(Mg + Fe) for olivine; Fs and Wo are afu 100 × Fe/(Mg + Fe + Ca) and 100 × Ca/(Mg + Fe + Ca) for pyroxene respectively. Al[#] is afu 100 × Al/(Al + Cr) for spinel and pyroxene; Mg[#] is afu 100 × Mg/(Mg + Fe) for spinel, olivine, and pyroxene; and Ti[#] is afu 100 × Ti/(Al + Ti) for spinel and pyroxene. Fe/Mn is afu Fe/Mn for olivine and pyroxene. All data are expressed as mean ± standard deviation except for very low levels of data. The standard deviation of these data is greater or equal to the average value, and they are unhelpful for scientific purposes.

and troctolites (mixture of mafic minerals + silicon glass + fine-grained plagioclase) was carried out using the Laser Ablation ICP-MS (LA-ICP-MS) at the Institute of Geochemistry, Chinese Academy of Sciences. Laser sampling was performed using a GeolasPro laser ablation system that consists of a COMPexPro 102 ArF excimer laser (wavelength of 193 nm and maximum energy of 200 mJ) and a MicroLas optical system. An Agilent 7700 cx ICP-MS instrument produced the ions. The laser's spot size was 24 μm, and the frequency was 6 Hz. Trace element compositions of minerals were calibrated against various reference materials (BHVO-2G, BCR-2G, and BIR-1G) without using an internal standard. Each analysis incorporated a background acquisition of approximately 20–30 s, followed by 50 s of data. The raw count rate data, including uncertainty, concentration, and detection limit, were found using the ICP-MS DataCal software (Liu et al., 2008). The data are given in Table 3.

2.4. Mineral Phase Analysis

Minerals were identified by laser Raman spectroscopy using a Renishaw inVia spectrometer at the Guilin University of Technology. The spectrometer uses an Ar⁺ laser, peak wavelength 780 nm, at 20 mW, with light directed through a microscope to a spot smaller than 1 μm diameter on a thin section. Scattered photons, with Raman, shifts from 100 to 1,300 cm⁻¹, were collected through the microscope into the spectrometer, which has a spectral resolution of 1 cm⁻¹. Spectra were calibrated against the 520.7 cm⁻¹ Raman shift scatter of metallic silicon.

3. Results

3.1. Petrography and Mineralogy

The NWA 12279 meteorite is nearly round and has typical atmospheric ablating and impact metamorphic characteristics. The prominent melting lines and the tan melting crust can be seen along the nearside of the flight direction. The rupture surface is grayish-white. The shrinkage cracks, impact gas marks, and impact melt are seen on the far side (Figure 1).

The fresh-cut surface comprises ~95 vol.% pristine holocrystalline magmatic rock and ~5 vol.% impact melt. Gemmy, equant grains of pink spinel are distributed randomly in matrix material mainly consisting of off-white plagioclase (Figure 2). The impact veins extending in the same direction are visible in this section (Figure 2a), indicating that NWA 12279 was sputtered away from the Moon after a directional impact. It did not undergo a complex process of multiple impacts. This unbrecciated rock comprises PST and presumed FANs xenoliths (coarse-grained plagioclases ± minor olivines, poikilitic texture). Under an orthogonal polarizing microscope, the coarse-grained plagioclases have significant optical characteristics, such as colorless and transparent, low positive protrusion, parallel extinction, and interference first order yellow color (Figure 2b), indicating that the impact metamorphic change degree is low. The mineral assemblage consists mainly of plagioclase (~82 vol.%), olivine (~12 vol.%), pyroxene (~3.5 vol.%), Mg-spinel (~1.2 vol.%), silica phase (~1.0 vol.%), and minor glass, Fe-Ni alloy with an average statistical data set of three thin sections by principal components on element X-ray maps from TIMA (Table 1 and Figure 2c). The spinel is dark red in a plane-polarized microscope, and cracks caused by impact can be seen on its surface. Plagioclase is divided into coarse-grained mass and fine-grained long strips. The tan matrix fills between the plagioclase in a plane-polarized microscope (Figure 2d). According to the relative content

Table 3
Trace Elements in the Minerals, Troctolite, and Whole Rock of Northwest Africa 12279 (ppm)

Samples	Whole rock	Coarse-grained plagioclase (<i>n</i> = 5)	Troctolite (<i>n</i> = 21)	Spinel (<i>n</i> = 7)
Analytical method	ICP-MS	LA-ICP-MS	LA-ICP-MS	LA-ICP-MS
Li	N. A.	2.97 ± 0.44	2.38 ± 0.65	B. D.
Sc	N. A.	1.16 ± 0.56	7.14 ± 4.94	1.16 ± 0.65
V	21.90	3.11 ± 0.71	19.77 ± 6.85	380.03 ± 11.60
Cr	873.59	42.74 ± 32.31	580.14 ± 209.49	N. A.
Co	21.45	1.36 ± 0.52	15.91 ± 8.64	110.06 ± 4.18
Ni	97.84	22.11 ± 13.93	41.66 ± 19.67	475.27 ± 138.61
Cu	4.64	0.74 ± 0.27	1.80 ± 0.79	1.36 ± 0.69
Zn	36.16	1.58 ± 0.45	2.91 ± 1.16	20.40 ± 2.32
Ga	8.41	B. D.	B. D.	21.89 ± 1.09
Rb	1.03	0.61 ± 0.24	0.32 ± 0.13	B. D.
Sr	165.51	176.14 ± 11.60	88.60 ± 14.33	16.47 ± 19.70
Zr	8.82	0.85 ± 0.55	6.98 ± 7.27	1.03 ± 1.52
Nb	0.84	0.06 ± 0.05	0.49 ± 0.60	B. D.
Ba	198.19	37.05 ± 25.70	31.84 ± 19.80	B. D.
Hf	0.32	0.02 ± 0.01	0.18 ± 0.17	0.02 ± 0.02
Ta	0.05	0.01	0.04 ± 0.04	B. D.
Th	0.15	0.02 ± 0.02	0.06 ± 0.05	B. D.
U	0.06	0.01	0.02 ± 0.01	B. D.
La	1.29	0.57 ± 0.29	0.46 ± 0.30	B. D.
Ce	2.85	1.39 ± 0.75	1.23 ± 0.84	B. D.
Pr	0.43	0.18 ± 0.10	0.17 ± 0.12	B. D.
Nd	1.76	0.55 ± 0.33	0.84 ± 0.66	0.2 ± 0.3
Sm	0.51	0.13 ± 0.08	0.28 ± 0.22	B. D.
Eu	0.79	0.75 ± 0.10	0.37 ± 0.08	B. D.
Gd	0.64	0.12 ± 0.07	0.38 ± 0.32	B. D.
Tb	0.10	0.03 ± 0.02	0.06 ± 0.05	B. D.
Dy	0.79	0.16 ± 0.09	0.45 ± 0.36	B. D.
Ho	0.18	0.03 ± 0.02	0.09 ± 0.08	B. D.
Er	0.54	0.09 ± 0.06	0.27 ± 0.23	B. D.
Tm	0.07	0.01 ± 0.01	0.04 ± 0.04	B. D.
Yb	0.48	0.08 ± 0.05	0.28 ± 0.24	B. D.
Lu	0.08	0.02 ± 0.01	0.04 ± 0.03	B. D.
Y	4.86	0.35 ± 0.22	2.54 ± 2.24	B. D.

Note. B. D. means below detection and N. A. means not applicable. Data are expressed as mean ± standard deviation.

of plagioclase, olivine, and pyroxene, NWA 12279 meteorite is classified as a troctolitic anorthosite (Figure 3, Gross et al., 2020). This paper defines it as pink spinel troctolitic anorthosite (PSTA) according to the uniformly distributed phenocrystic spinels. PSTA is defined for the first time in this article.

NWA 12279 meteorite has a holocrystalline, porphyritic-like, and interstitial texture. In addition, some FAN xenoliths have a poikilitic texture. The particle size of spinel is much larger than that of olivine and pyroxene interstitials, forming a porphyritic-like texture. This indicates that there are noticeable differences in their forming environments. The euhedral spinels are randomly distributed in the troctolitic matrix. No particle-sized spinel was found in the melt veinlets (Figure 4a). The above phenomenon indicates that the formation of pink spinel in

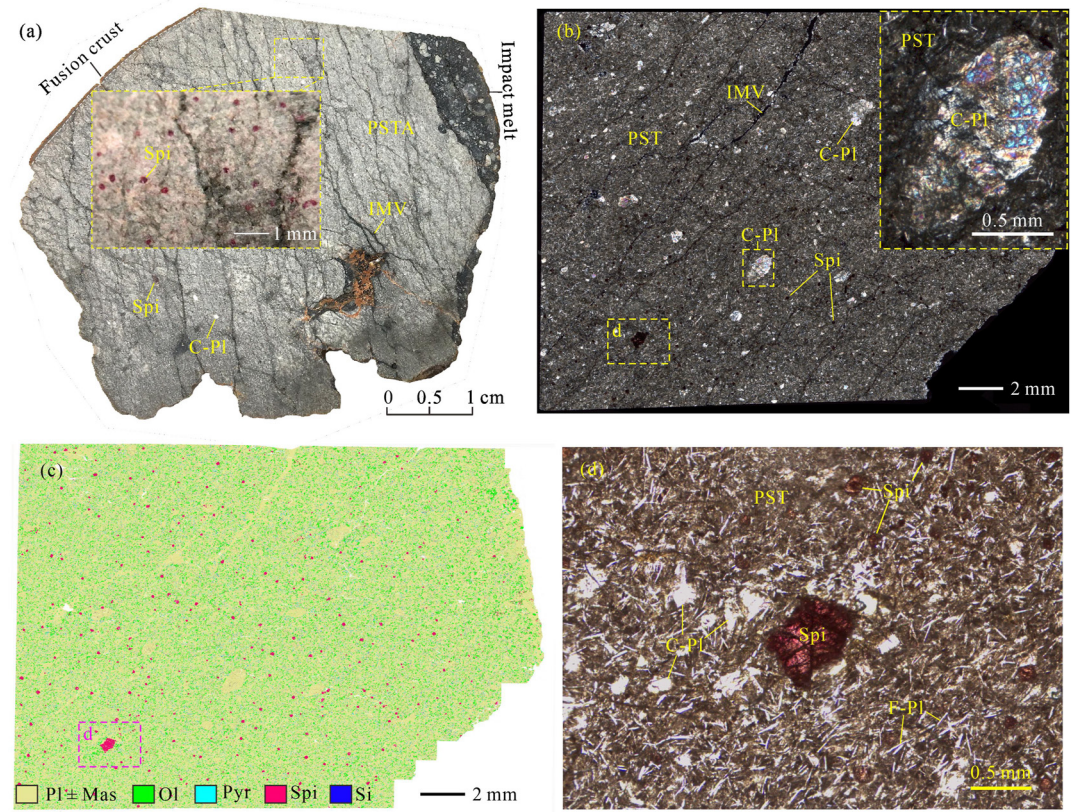


Figure 2. The macroscopic view of the fresh cutting surface and the microscopic mosaic images of a polished section Northwest Africa 12279, 2. (a) The macroscopic views of the fresh cutting surface. It shows that the pink spinel phenocrysts are embedded uniformly in the light gray troctolitic matrix. (b) Cross-polarized light mosaic image. Millimeter plagioclase xenolith and submillimeter spinel phenocrysts can be clearly seen. (c) The elemental x-ray map. (d) The plane-polarized light image. C-Pl—Coarse-grained plagioclase, F-Pl—Fine-grained plagioclase, IMV—Impact melt veinlet, Mas—Maskelynite, Ol—Olivine, Pyr—Pyroxene, PST—Pink spinel troctolite, PSTA—Pink spinel troctolitic anorthosite, Spi—Mg-spinel, and Si—Silica phase.

NWA 12279 has nothing to do with the shock-melt veinlets. The “Olivine ± pyroxene ± silica-rich glass” assemblage fills in a triangular or rhombic gap of the fine lath-shaped plagioclase to form an interstitial structure. The combination between pyroxene and silica-rich glass occurs as an intertwined graphic texture. In contrast, isolated olivine occurs as a subhedral and anhedral (Figure 4b). Low-Ca pigeonite is homogeneous in composition and has distinct boundaries from needle-like high-Ca augite (Figure 4c). Plagioclases occur as euhedral to subhedral lath-shaped fine grains in the troctolite. Most fine-grained plagioclases have been converted into maskelynite by impact. The coarse-grained plagioclases occur as xenoliths in the troctolite. They encase some olivines to form a poikilitic texture (Figure 4d).

The Mg-spinels occur as euhedral grains in troctolite. Most spinel sizes are 100–200 μm (Figure 2). The largest one is 750 \times 550 μm (Figures 2 and 4e). Five hundred sixty spinels larger than 100 μm were investigated in three polished thin sections, and 38 contained magma melt inclusions (Table 1). These inclusions generally exhibit an immiscible separation of the liquid phase, which can be divided into a magnesium-rich and silica-rich phase (Figures 4f–4h). The ratio (vol.%) of the Mg- and Si-rich phases is 4:1–10:1. Some of the Si-rich phases contain taenite beads (Figure 4g) and occur as worm-like scattered in the Mg-rich phase (Figure 4h). Two distinct phases can be seen in the peanut-shaped melt inclusions of olivine. One phase is a Si-rich melt with quartz. The other consists of needle-like crystalline high-Ca augite and silica glass. The area of the Si-rich melt is more significant than that of the Mg-rich phase (Figure 4i). The needle-like high-Ca augite of the inclusion has the same morphology as the pyroxene filled in the gap of plagioclase (Figures 4c and 4i).

Based on a laser Raman spectrum analysis, all olivines, some pyroxenes, and a small amount of quartz is crystallized and form an anhedral crystal. Many of the pyroxenes present micron skeletal crystals interwoven with

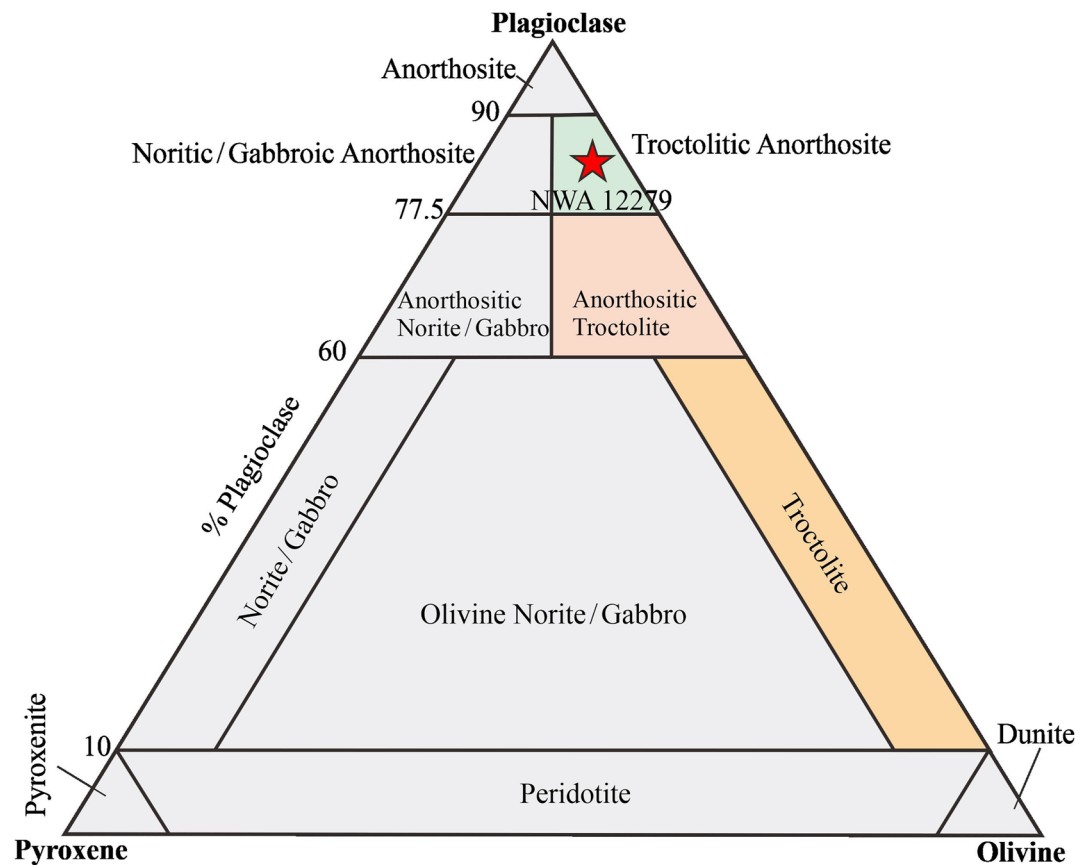


Figure 3. Lithologic classification of the Northwest Africa (NWA) 12279 meteorite. This figure shows the troctolitic suite spanning from the troctolitic anorthosite (green-shaded fields) to the anorthositic troctolite and the troctolite (Gross et al., 2020). The red star represents NWA 12279.

a glass matrix. Among 30 analysis points of this silicon phase, only one is consistent with the characteristics of quartz. The rest are all silica-rich glass. The coarse-grained plagioclase has diagnostic Raman spectral peaks, indicating that it has suffered low-impact metamorphism (Figure 5).

3.2. Minerals, Inclusions, and the Bulk Compositions

Different mineral grains (including spinel, olivine, and pyroxene) in the PST of NWA 12279 (except for plagioclase xenocrysts) do not have homogeneous chemical compositions. But the chemical composition of a single spinel is relatively uniform. There are no noticeable changes regularly from cores to rims (Figure 6a), or the core is slightly rich in magnesian than their rims (from 85.6 to 84.7, Figure 6b). Different spinel grains show a range of compositions: $Mg^{\#} = 70.3\text{--}85.7$, $Al^{\#} = 89.0\text{--}99.1$, and $Cr^{\#} = 0.91\text{--}11.0$. Different cores of spinels have almost the same composition (mean \pm standard deviation, 85.5 ± 0.81), and the component of rims have slightly more significant variation (avg. 77.6 ± 3.87) (Table 2). EPMA analyzed the components of 22 spinels from core to rim. We found that the chemical composition zonation of spinel is not apparent. The mean range of variation of $Mg^{\#}$ from core to rim in the same spinel particle is less than 1 (Figure 7).

The “olivine \pm pyroxene \pm silica phase” assemblages fill the rhomboid or triangular void of plagioclase. Olivine grains have relatively magnesian cores ($Mg^{\#} = 88.5$) and fewer magnesian rims ($Mg^{\#} = 78.6$). Pyroxene grains surround the edge of olivine, and its $Mg^{\#}$ (71.3) is lower than that of olivine. The silica phase is distributed in clumps along the sides of the pyroxene (Figure 8). Many olivine composition statistics showed that the core of olivine was relatively rich in magnesium ($Mg^{\#}$, 80.4 ± 3.35), and the rim was relatively poor in magnesium ($Mg^{\#}$, 73.8 ± 6.09). The $Mg^{\#}$ of olivine grains (excluding the xenocrysts in coarse-grained plagioclase) have a relatively large range of variation ($Mg^{\#}$, 53.9–83.3, Figure 9a, Table 2).

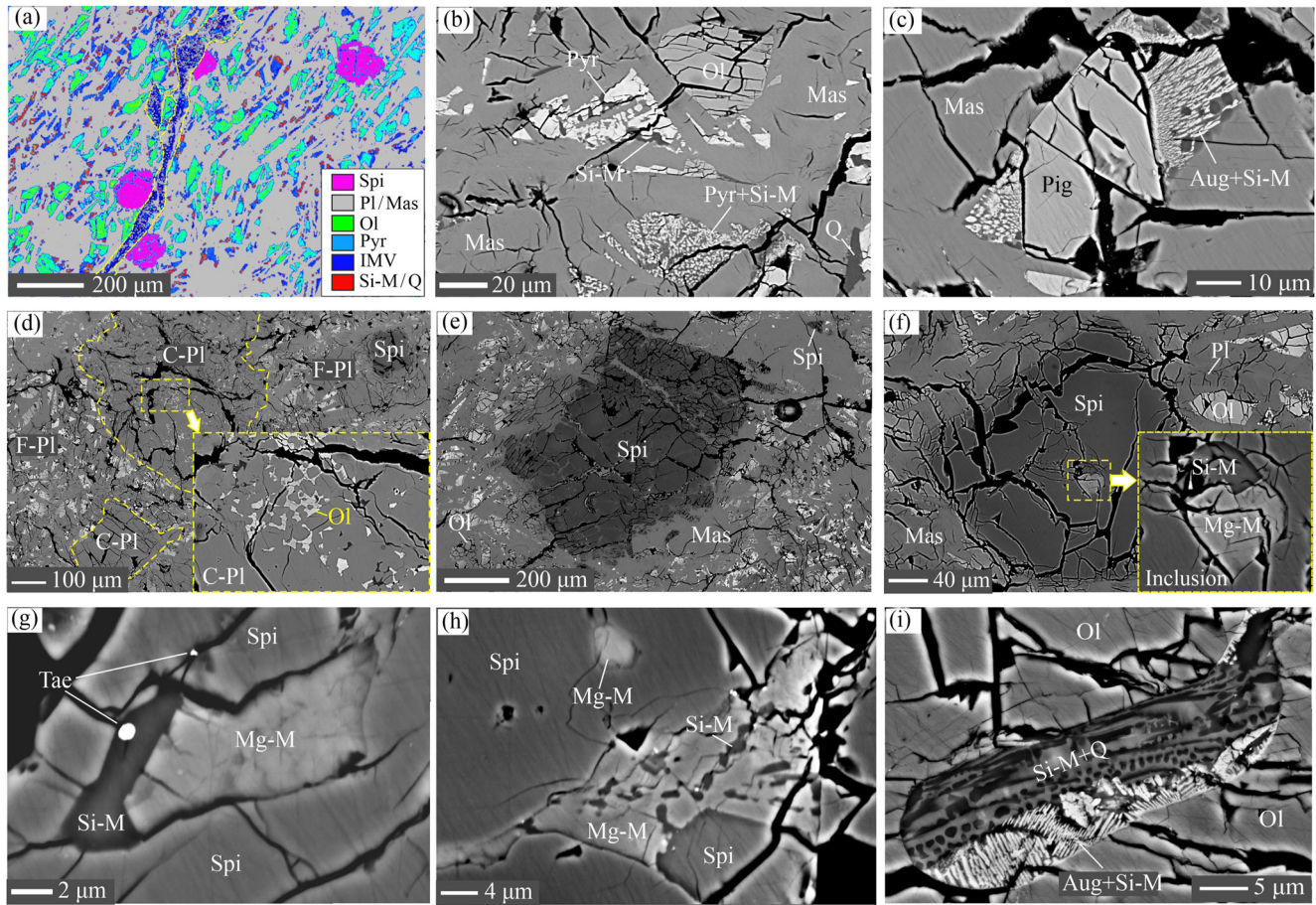


Figure 4. Microtextures in Northwest Africa 12279, 2. (a) X-ray elemental map of the Mg-spinel assemblages. (b) Olivine, pyroxene + silica phase assemblages fill the gaps of lath-shaped plagioclase. They form an interstitial structure. (c) Low-Ca pigeonite in the core and high-Ca augite + Si-rich melt in the rim, filling the plagioclase gap. (d) A coarse-grained plagioclase xenolith is wrapped in pink spinel troctolites. Anhedral olivine is embedded in the plagioclase to form a poikilitic texture. Similar textures and mineral assemblages have been found in lunar Ferroan Anorthosites (Walker & Hays, 1977). (e) A large-grained spinel with a size of $750 \times 550 \mu\text{m}$. Its uniform gray level implies the consistency of chemical composition. (f) The magma melt inclusion in the spinel exhibits a liquid phase immiscible separation. (g) The “Mg-rich phase + Si-rich phase + taenite” assemblage is melt inclusion of spinel. (h) A worm-like Si-rich melt of inclusion in the spinel. (i) The melt inclusion in olivine comprises the silica-rich melt + quartz and pyroxene + silica-rich melt. (b–i) are Backscattered electron images. Aug–Augite, C-Pl–Coarse-grained plagioclase, F-Pl–Fine-grained plagioclase, IMV–Impact melt veinlet, Mas–Maskelynite, Mg-M–Mg-rich melt, Ol–Olivine, Pl–Plagioclase, Pyr–Pyroxene, Pig–Pigeonite, Q–Quartz, Spi–Spinel, Si-M–Si-rich melt, and Tae–Taenite.

The $\text{Mg}^\#$ of Mg-rich melt inclusions was significantly higher than that of spinel as the parent. Generally speaking, Mg-rich melt inclusions in the spinels have a high $\text{Mg}^\#$ (71.8–90.5, avg. 82.4), while those with olivine are relatively low ($\text{Mg}^\#$, 49.3–71.8, avg. 58.4). In the order of the average $\text{Mg}^\#$ value from high to low, the mafic minerals or melt are Mg-rich melt inclusions and spinels (82.4), olivines (76.9), and pyroxenes (58.4). Mg-rich inclusions in the spinel and the spinel share the same average $\text{Mg}^\#$ value (82.4). However, the $\text{Mg}^\#$ has overlapped in different minerals and melt inclusions (Figure 9a).

Pyroxene grains show a similar pattern, ranging from magnesian augite to ferroan augite and pigeonite (Figure 9b). The average $\text{Mg}^\#$ of pyroxene (33.6–74.2, avg. 58.0) was lower than that of olivine (53.9–79.1, avg. 73.4). The range of variation is more significant than that of olivine (Table 2). The variation in plagioclase compositions is insignificant ($\text{An}_{92.2-97.7}$). We do not have data on plagioclase zoning. On the other hand, the xenolithic plagioclase grains have a relatively more restricted range of compositions ($\text{An}_{95.2-98.7}$, avg. 97.6) than that in the troctolite host: $\text{An}_{92.2-97.7}$, avg. 95.2 (Figure 9c).

The Fe-Ni alloy is mainly taenite (Ni, 27.5–59.9 wt.%; Co, 0.40–2.46 wt.%), followed by kamacite (Ni, 15.7–26.2 wt.%; Co, 0.87–1.54 wt.%). There is an inverse correlation between the contents of $\text{Na}_2\text{O} + \text{K}_2\text{O}$ and $\text{MgO} + \text{FeO}$ (wt.%) of Si-rich and Mg-rich melt inclusions. Si-rich melt inclusions have the highest $\text{Na}_2\text{O} + \text{K}_2\text{O}$ content of all phases in NWA 12279. Their compositions overlap the Mg-rich melt inclusions, pyroxenes, and

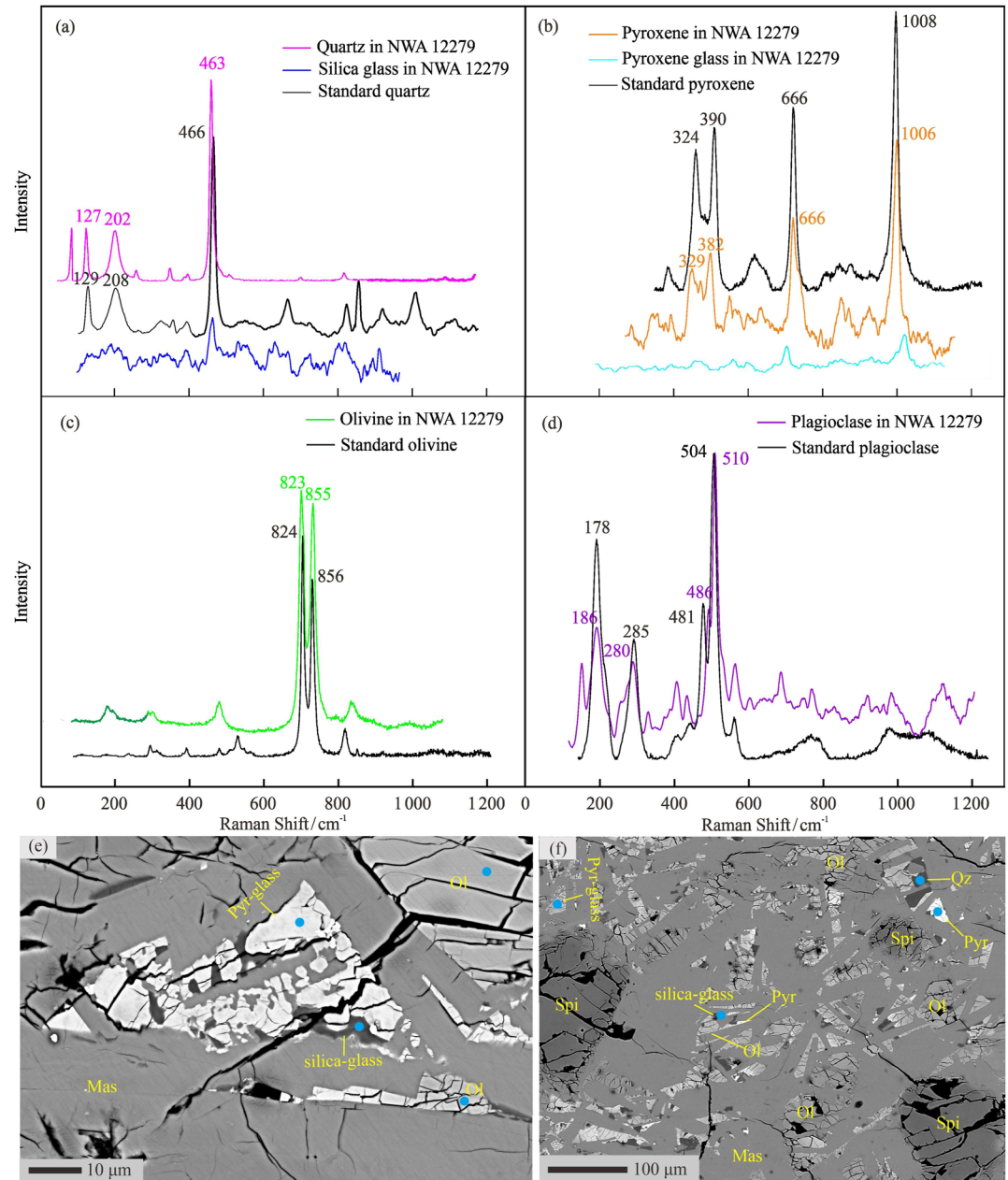


Figure 5. Raman spectra of minerals and glass, and corresponding Backscattered electron (BSE) images of Northwest Africa 12279, 3. The standard spectra data come from the RRUFF Database (<https://rruff.info/>). The solid blue dots are the positions analyzed by Raman spectroscopy. (a) Quartz and silica glass. (b) Pyroxene and pyroxene glass. (c) Olivine. (d) The coarse-grained plagioclase xenolith. (e, f) are the BSE images corresponding to the analysis positions of the Raman spectra. Mas–Maskelynite, Ol–Olivine, Pyr–glass–Pyroxene glass, Pyr–Pyroxene, Qz–Quartz, and Spi–Mg-spinel.

spinel. The bulk composition is consistent with the weighted average of Si-rich and Mg-rich melt inclusions and plagioclases (Figure 10a). The bulk Mg[#] and Al₂O₃ (wt.%) content of Mg-rich melt inclusions are consistent with the trendline of peridotites from the lunar mantle (Dymek et al., 1975). The Mg[#] of the whole rock is in the range of Mg-suite (Figure 10b). Detailed data are shown in Table 2.

3.3. Trace Elements

The contents of Cr, Ni, and Co in olivine, whole rock, and troctolite host of NWA 12279 are consistent with those in the lunar Mg-suite lithologies of ultramafics, troctolites, and PST. They are different from norites

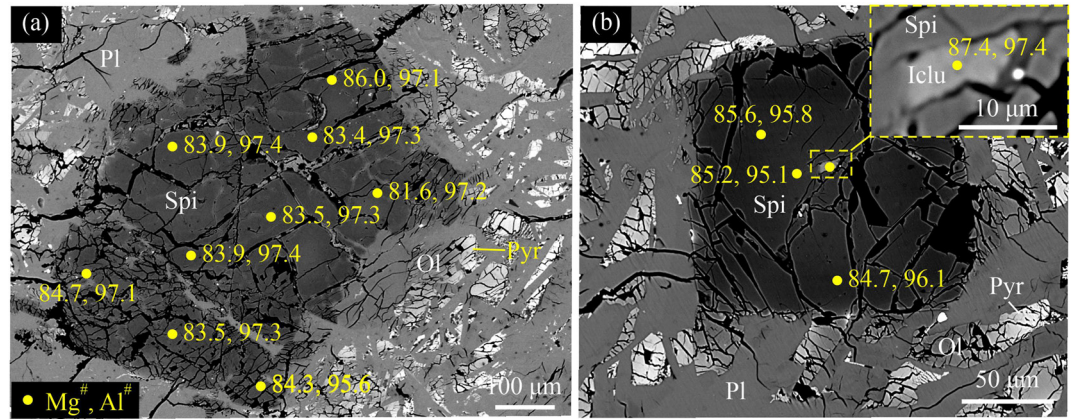


Figure 6. The composition distribution of Mg-spinel and its molten magma inclusion in Northwest Africa 12279, 2. (a) The largest spinel and its composition. (b) Representative spinel and its inclusion composition. Iclu—Magma molten inclusion, Ol—Olivine, Pyr—Pyroxene, Pl—Plagioclase, and Spi—Mg-spinel.

and mare basalts (Figures 11a and 11b). The distribution of Fe and Mn in olivine and pyroxene is consistent with that of lunar meteorites and Apollo samples (Figure 11c). The distribution of Y and Ba elements in the coarse-grained plagioclase is consistent with FANs from the Apollo samples. In contrast, the distribution of Y and Ba in fine-grained plagioclase of troctolite host rock in NWA 12279 is consistent with Mg-suite lithologies (Figure 11d). The REE pattern of the whole rock and PST in NWA 12279 is flat. The fractionation between light and heavy REEs is not apparent. Positive Eu anomalies are observed in whole rock, coarse-grained plagioclase, and troctolite host (Figure 12a). The distribution of the incompatible elements in the whole rock and PST is consistent with that of lunar troctolite, except for the K and Cs (Figure 12b). Detailed data are shown in Table 3.

4. Discussion

4.1. Lunar Origin and Primitiveness of NWA 12279 Meteorite

NWA 12279 is a newly recovered meteorite with typical characteristics of atmospheric ablation (Figure 1). Its mineral assemblage and composition are similar to that of lunar PST (Gross & Treiman, 2011; Marvin et al., 1989; Wittmann et al., 2019). The texture and compositions of plagioclase xenoliths therein are similar to highland FANs (Figures 4d and 9c). The Fe/Mn ratio of mafic minerals is widely used as a characteristic “fingerprint” for planetary bodies (Papike, 1998). The ranges of Fe/Mn ratio for olivine and pyroxene of NWA 12279 are consistent with the literature for lunar meteorites and Apollo samples (Figure 11c). These pieces of evidence confirm that

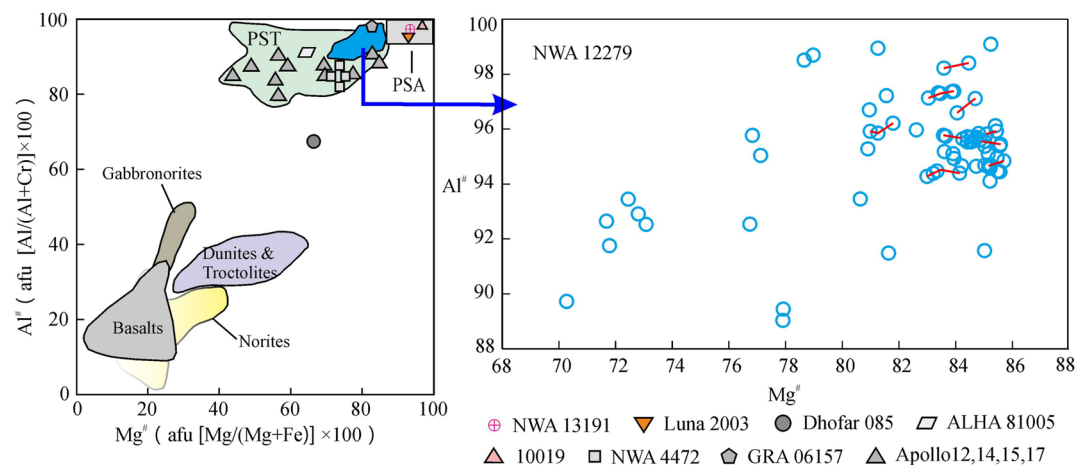


Figure 7. The plot of Mg# versus Al# for spinels in Northwest Africa 12279 (solid blue area, the detailed image on the right). The red line represents an independent spinel crystal). It is compared to literature for lunar meteorites, Apollo samples, and M³ remote sensing (Gross, Isaacson, et al., 2014; Jackson et al., 2014; Prissel et al., 2014, 2016; Wittmann et al., 2019).

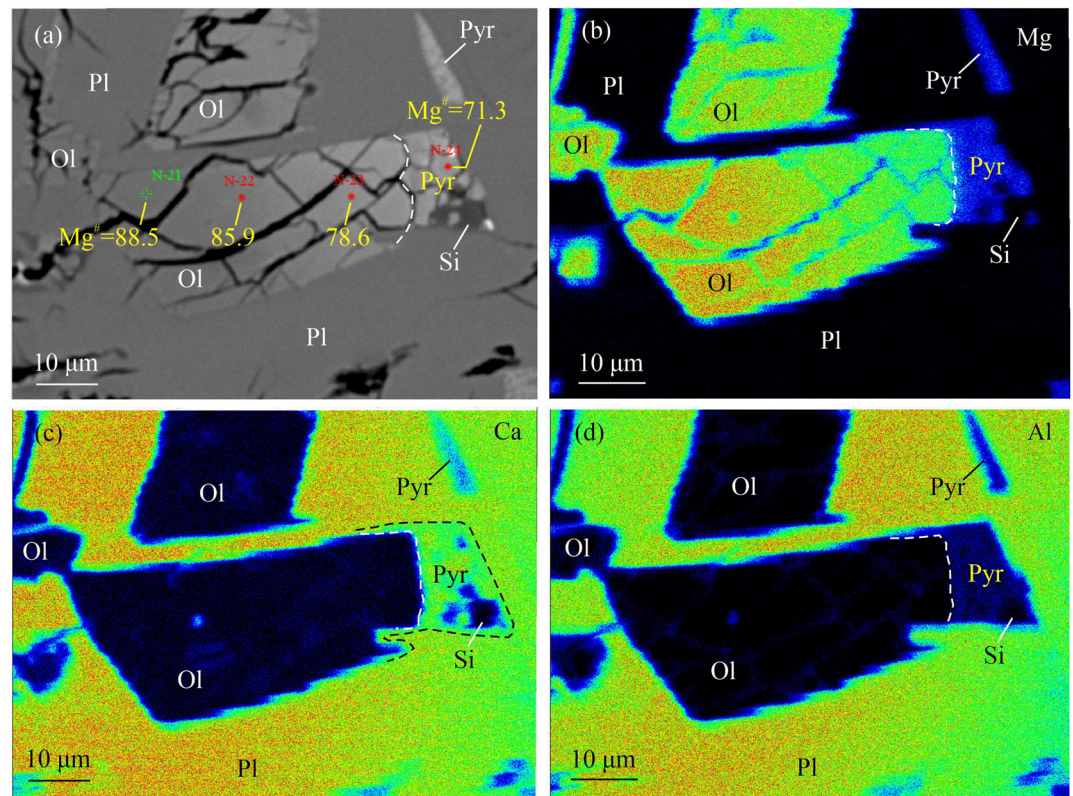


Figure 8. The composition distribution of olivine and pyroxene in Northwest Africa 12279, 2. (a) Backscattered electron image; (b–d). Elemental X-ray mappings of Mg, Ca, and Al, respectively. Warm colors indicate relatively high element content. N-21—N-24 are analysis point position and original number. Ol—Olivine, Pyr—Pyroxene, Pl—Plagioclase, and Si—Silica phase.

NWA 12279 meteorite originates from the highland of the Moon. NWA 12279 is a rare meteorite with a complete melting crust, clear flow lines, impact gas mark, and shrinkage crack (Figure 1). Such a Saharan lunar meteorite is unique, and these features suggest that NWA 12279 could have landed recently and therefore had very low terrestrial weathering. As a result, NWA 12279 meteorite provides raw information about the evolution of lunar magma.

NWA 12279 is an important and unique lunar meteorite as it is both unbrecciated and pristine. PST host rock (spinel phenocryst + troctolite) and FANs xenolith constitute nearly all the mass (1,830 g, ~95 vol.%) of a large solid chunk. They show consistent phenocrystic and interstitial textures (Figure 2). The $Mg^{\#}$ of the whole rock is consistent with that of the Mg-suite or magnesian anorthosites (MANs) from Apollo samples and lunar meteorites. The range of $Mg^{\#}$ of the Mg-rich melt inclusions must be consistent with the trendline of the peridotite from the plutonic ultramafic member of the Mg-suite or mantle material (Figure 10b). While plutonic ultramafic Mg-suite is formed by partial melting of the lunar mantle (Shearer et al., 2015). The Apollo 72415 dunite as a plutonic ultramafic Mg-suite or mantle material is a reasonable assumption. It is one of the oldest lunar rocks (4.51 ± 0.10 Gyr with Rb–Sr dating or 4.37 – 4.52 Gyr with U–Pb dating) (Papanastassiou & Wasserburg, 1975; Premo & Tatsumoto, 1992). It comprises 93% olivine (coarse-grained olivine embedded in fine-grained olivine matrix), 4% plagioclase, and 3% pyroxene. Although the Mg-rich olivine-bearing mantle is consistently not plagioclase saturated in both experimental and simulations of LMO crystallization, the Apollo dunite 72415 contains a small amount of plagioclase. However, the lunar crust is mainly composed of plagioclase. Understandably, the mantle-derived rocks from the shallow part of the lunar mantle to the crust-mantle joint part contain a small amount of plagioclase. Dunite 72415 is also believed to be an early crystallization from LMO and may represent the lunar mantle composition (Dymek et al., 1975). It is also one of the most magnesian ($Mg^{\#} = 89$) rocks from the Moon (Wang et al., 2015). The $Mg^{\#}$ of whole rock (87.9 ± 0.68), Mg-rich melt inclusions in spinels ($Mg^{\#}$, 82.4 ± 4.57), and Dunite 72415 share a similar compositional trend (Figure 10b), suggesting that they are genetically related.

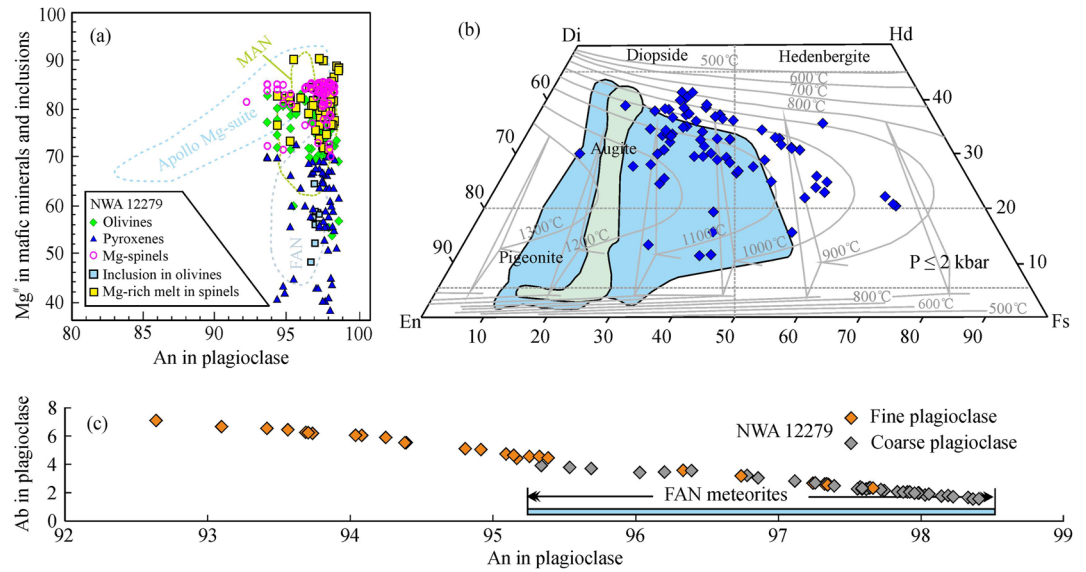


Figure 9. Variation trends of different minerals and inclusions in Northwest Africa (NWA) 12279. (a) Mg[#] in mafic minerals and melt inclusions versus An in coexisting plagioclase for NWA 12279. The composition fields of Apollo Mg-suite, Ferroan Anorthosites (FANs), and magnesian anorthosites are from the literature (Gross, Treiman, & Mercer, 2014; Lindstrom et al., 1989). (b) Quadrilateral diagram of pyroxene. Temperature contours calculated at <2 kbar (Lindsley & Andersen, 1983) are shown, where that value was chosen according to the possible pressure range (<40 km) for lunar pink spinel troctolites. The depth was calculated using the average lunar lithostatic gradient of 0.05 kbar/km (Herzberg & Baker, 1980). The lunar olivine-bearing Mg-suite (light blue area) (Shearer et al., 2015) and NWA 2996 noritic and troctolitic anorthosite clasts (light green area) (Mercer et al., 2013) are plotted for comparison. Di, diopside; En, enstatite; Fs, ferrosilite; and Hd, hedenbergite. (c) The compositions of plagioclase (Ab = molar, [Na/(Ca + Na + K)] × 100). The solid blue line represents the range of values in FANs from the literature (Xu et al., 2020).

The contents of the siderophile elements (e.g., Co, Ni) of the whole rock, Cr in olivines, and troctolites are consistent with the Apollo ultramafics, troctolites, and PST. However, they are different from the norite and mare basalts, which are highly evolved. The bulk Co/Ni ratio (0.22) is much greater than the ratio (0.05) of the

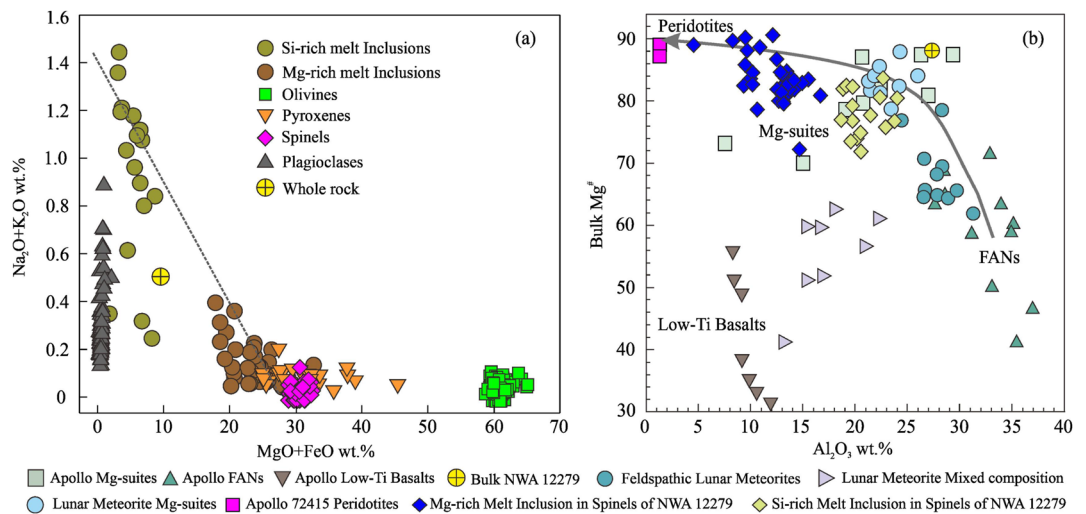


Figure 10. Main compositions of magma melt inclusions, minerals, and whole rock in Northwest Africa (NWA) 12279 compared to different lunar lithologies. (a) Na₂O + K₂O, wt.% versus FeO + MgO, wt.% of melt inclusions in the spinels and minerals of NWA 12279. (b) Bulk molar Mg[#] versus Al₂O₃ content for NWA 12279 compared to the literature data (Gross et al. (2020) and references therein). The solid gray arrow is mixing between ferroan anorthosite and the magnesian anorthositic granulite average or hypothetical magnesian peridotite by Apollo 72415 (representing the lunar mantle, Dymek et al., 1975).

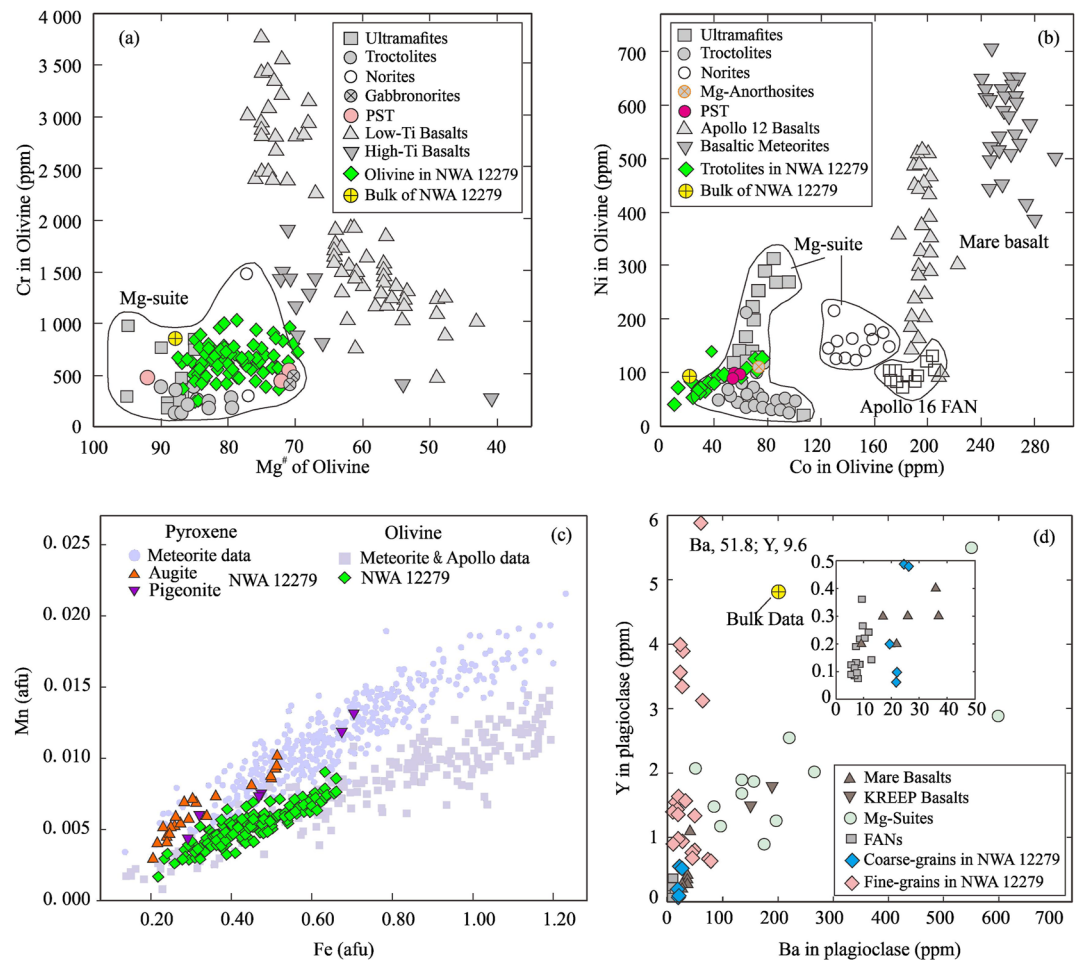


Figure 11. Trace element compositions of olivine, pyroxene, and plagioclase in Northwest Africa (NWA) 12279 compared to the mineral assemblages from different lunar lithologies. (a) Cr versus Mg[#] in parts per million (ppm) of olivine and the whole rock from NWA 12279 (solid green rhombus) compared to olivine from Mg–suite lithologies and mare basalts (Shearer et al., 2015). (b) Ni versus Co of troctolites and whole rock from NWA 12279 (solid green rhombus) compared to olivine from Mg–suite lithologies, Ferroan Anorthosites, and mare basalts (Shearer et al., 2015). (c) Mn versus Fe in olivine (solid green rhombus) and pyroxene (solid orange and purple triangles) of NWA 12279 compared to the literature for lunar meteorites and Apollo samples (Gross et al., 2020). (d) Y versus Ba in plagioclase (the pink and blue solid rhombus) of NWA 12279 compared to the literature (Papike et al., 1996; Shearer & Papike, 2005; Shervais & McGee, 1998, 1999).

chondritic meteorites (Warren, 1993). Most iron-nickel alloys are taenite, not kamacite, commonly found in the chondrite. The distribution pattern of REEs and the incompatible elements for the whole rock are consistent with those of the Apollo Mg-suite and troctolites, which differ from those of KREEP-bearing clasts and FANs (Figure 12). These indicate that NWA 12279 is little modified by the impact mixing of meteorites. Therefore, the primitiveness of NWA 12279 is at a confidence level of 9 (highest degree) according to Warren (1993)'s criteria. NWA 12279 meteorite can provide direct evidence for the petrogenesis of Mg-suite represented by PST or PSTA. We use this observation as a foundation to examine the early lunar crust-mantle interaction.

4.2. The Formation of Spinel Is a Result of Interaction Between the Early Lunar Mantle Melt and Crust

The model that the parent magma of Mg-suite originated from the lunar mantle depressurized melting is a reasonable assumption (Prissel & Gross, 2020; Shearer et al., 2015). In magmatic systems such as the lunar troctolitic parent, Mg-spinel and Mg-rich olivine have the highest liquidus and are to crystallize firstly from the melt (Prissel et al., 2016). The range of Mg[#] of the Mg-rich melt inclusions is consistent with the trendline of the peridotite from the lunar mantle or plutonic ultramafic Mg-suite (Figure 10b). So, the magma melt inclusions trapped in the spinels may originate from the lunar mantle melt contaminated by crust anorthosite. The chemical composition

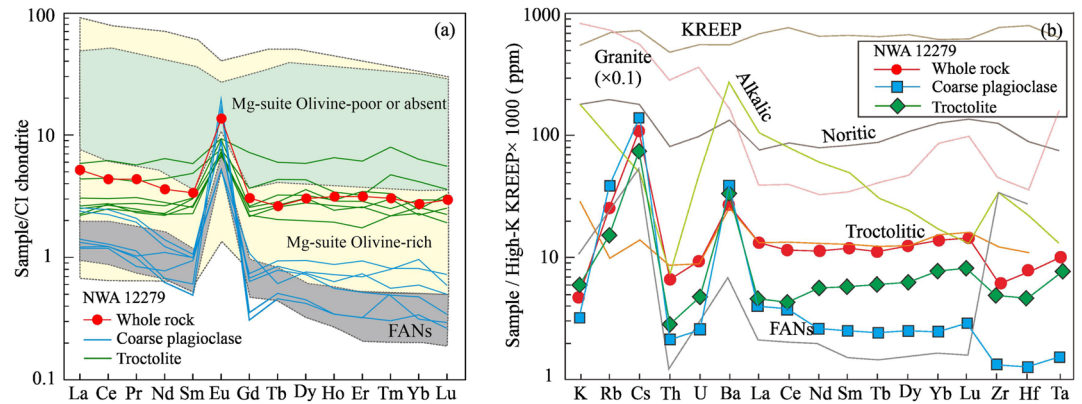


Figure 12. Trace element distribution. (a) Rare earth element (REE) distribution of whole rock, coarse-grained plagioclase, and troctolite in Northwest Africa (NWA) 12279. CI chondrite values are from the literature (Anders & Grevesse, 1989), the REE range is from the Apollo Ferroan Anorthosites (FANs) (Floss et al., 1998; Papike, 1998), the Mg-suite olivine-rich, and the Mg-suite olivine-poor or absent (Shearer et al., 2015) are shown as a gray, yellow, and green-shaded area, respectively. (b) Compared to the literature data (Warren (1993) and references therein), there is an incompatible trace element pattern for the whole rock, FANs xenolith, and the troctolite main body in NWA 12279.

of spinel is uniform, but the chemical composition of olivine and pyroxene are inhomogeneous, and the absence of exsolution bands in the pyroxene (Figures 4c and 8) indicates a low degree of thermal metamorphism for NWA12279. Therefore, the homogeneous composition of the spinel could not have been formed by chemical re-equilibration but by a balanced crystallization product. Equilibrium crystallization of a spinel on the Moon can only be achieved in the lower crust, crust-mantle boundary, or mantle, where the temperature can slowly decrease.

The global distribution of PSA on the lunar surface has rekindled scientists' enthusiasm for determining the spinel-bearing lithologies (Gross & Treiman, 2011; Gross, Isaacson, et al., 2014; Pieters et al., 2014; Prissel & Gross, 2020; Prissel et al., 2014, 2016; Shearer et al., 2015; Sun et al., 2017). Possible explanations for the petrogenesis of these lithologies range from low-pressure near-surface crystallization to high-pressure of the lower mantle. Three major hypotheses have been proposed: (a) Impact metamorphism, Mg-spinels formed at low pressure from the impact melting of Mg-rich anorthosite (Treiman et al., 2010). The enthalpy constraints from Treiman et al. (2019) suggest that the presence of spinel anorthosite on the crater and central peak results from rapid cooling and partial crystallization of super liquidus melts produced in the impacts and not from uplift of lower mantle material to the Moon's surface. An experiment on synthetic impact melt composition similar to Apollo PST 65785 crystallized a maximum of ~8 wt% spinel at 1 bar (Gross, Isaacson, et al., 2014). The genetic study of Mg-spinel-bearing clasts in NWA 13191 shows that the spinel was formed by the recrystallization of magnesia anorthosite after impact melting (Xie et al., 2023). (b) Contact metasomatic metamorphism, Mg-spinels formed at low pressure by a chemical reaction between Mg-rich magma and crustal anorthositic wall-rock (Gross & Treiman, 2011; Morgan et al., 2006). (c) Early magma-cumulated crystallization, Mg-spinels formed at high pressure in the lower mantle. These spinel-rich zones represent lower mantle materials excavated by impacts (Herzberg & Baker, 1980; Marvin et al., 1989; Wittmann et al., 2019).

The petrology, mineralogy, and geochemistry of NWA 12279 have supported and been confirmed by the hypothesis of a chemical reaction between Mg-rich magma (i.e., originate from magnesian plutonic rocks of the lunar lower mantle) and an anorthositic crust from the lower crust to near-surface at low pressure (Borg et al., 2020; Prissel & Gross, 2020; Prissel et al., 2014, 2016; Ryder, 1991; Simon et al., 2022; Warren, 1986). The energy of melting of magnesium-rich plutonite in the lower mantle is related to decompression melting, which itself is associated with the mantle overturn process (e.g., Borg et al., 2020; Elkins-Tanton et al., 2002; Gross et al., 2020; Prissel & Gross, 2020; Shearer et al., 2015). These hot Mg-rich melts then interact at the base of or within the lunar crust to form spinel-bearing melts. Then, these spinel-bearing continue to crystallize or ascend and crystallize to form troctolitic assemblages and spinel-bearing troctolites.

The primary evidence is as follows:

1. The large granular spinels (avg. 100–200 μm, max. ~750 × 550 μm) are evenly distributed in the troctolite of NWA 12279 (avg. 0.59 grains/mm² for greater than 100 μm spinels, Table 1 and Figure 2). The chemical

composition of spinel is relatively uniform. The compositional zonation is not apparent (Figures 6 and 7). The Mg[#] of spinel is between lunar PST and PSA defined by remote sensing (Gross & Treiman, 2011; Pieters et al., 2011). All these phenomena reflect the characteristics of the equilibrium crystallization for the crust-mantle boundary-mixed magma, as discussed above (Marvin et al., 1989; Wittmann et al., 2019). Similar cases include ~0.7 mm Mg-spinel crystals, Al-rich pyroxene, Mg-olivine, and cordierite from Dho 1528 lunar meteorite (Wittmann et al., 2019). Cordierite is also found in the Apollo collection, specifically within PST. It is not a stable phase in the liquid line of descent for Mg-suite melts, and its presence is more indicative of some secondary processing from Mg-spinel (Prissel et al., 2016). Olivine + plagioclase, or troctolitic assemblage, requires relatively low pressure (≤ 3 kbar or so), and on the Moon, this is restricted to most crustal pressures and depths (≤ 60 km) (Prissel et al., 2016). Olivine in NWA 12279 existing in the interstitial state has pronounced compositional zonation in some grains (Figure 8). Some pyroxene exists in the melt phase. Most of the silica-rich phase is not crystallized into quartz (Figure 5). These phenomena suggest that the “plagioclase + olivine + pyroxene” troctolitic combination is the product of unbalanced crystallization in a low-pressure near-surface. A comparison with compositions of Mg-spinel in lunar samples identifies a discrete range of chemical compositions equilibrated at depths > 25 km on the Moon (Wittmann et al., 2019). Therefore, the Mg-spinels ($> 100 \mu\text{m}$) in NWA 12279 may have formed in the lower lunar crust at depths > 25 km, while the “olivine \pm pyroxene \pm silica phase” troctolitic assemblage formed low-pressure near-surface on the Moon.

2. The magma melt inclusions in spinels and olivine occur as a liquid phase immiscible separation (Figures 4f–4i). Therein, the Mg-rich melts have the same compositional trend as the Mg-suite and the lunar peridotite (Figure 10b, peridotite trend is as described above). The content of siderophile trace elements of olivines, PST, and the whole rock in NWA 12279 is consistent with Mg-suite from lunar highlands (Figures 11a and 11b). Si-rich melts have the highest Na₂O + K₂O content of all phases (Figure 10a). This melt may have been the initial origin of the granitic rocks and alkali-norites of the lunar highlands (Shearer et al., 2015). It may have played a vital role in forming lunar “granitic” intrusive rocks (Yang et al., 2023).
3. Coarse-grained plagioclases have a similar texture and composition with Apollo and meteorite FANs (Figures 4d and 9c). The distribution of Y versus Ba (Figure 11d), REEs, and incompatible element pattern of coarse-grained plagioclases are consistent with FANs from Apollo and meteorites (Figure 12). Fine-grained lamellar plagioclases have relatively high content of Y and Ba, which is similar to the Mg-suite (Figure 11d). There is a clear boundary between coarse-grained plagioclase and troctolite (Figure 4d), suggesting they are FANs xenolith of the invading melt. Petrological and geochemical evidence suggests that the fine-grained plagioclases are recrystallized minerals after the magnesian melt invaded and incorporated the calcium feldspathic lunar crust.
4. As the main body of the sample, the troctolite has an interstitial structure similar to a diabase. “olivine \pm pyroxene \pm silica glass” assemblage is filled in the triangular or rhombic gap formed by lath plagioclase (Figures 2d and 4b). This formation is a significant feature of a hypabyssal magma intrusive rock. The crystallization temperature of pyroxenes is shown in Figure 9b and varies from 1300 to 800°C at $P < 2$ kbar (this pressure would be equivalent to lunar depths of < 40 km on the Moon) (Lindsley & Andersen, 1983). However, the temperature of pyroxenes in the olivine-bearing Mg-suite (Shearer et al., 2015), NWA 2996 noritic, and troctolitic anorthosite clasts (Mercer et al., 2013) are in the range of 1300–1000°C at depths of 20 km. Many pyroxenes in NWA 12279 occur as micron skeletal crystals and interweave with a glass matrix (Figures 4b and 4c). In addition, abundant silica and some pyroxene glasses can be found (Figure 5). These observations show that rapid quenching occurs in the late crystallization stage. The final cooling depth of troctolite in NWA 12279 may be near the surface of the Moon. Troctolite and mafic minerals in NWA 12279 have a primitive parental magma composition similar to Mg-rich mafic silicates (Figures 9a, 11a, and 11b). However, they have quite different REE patterns and abundances of incompatible trace elements from the evolved parental magma of some Mg-suites, for example, alkalic, noritic, granitic, and KREEP rocks. The distribution of incompatible elements in whole rock (the unbrecciated spinel-bearing troctolite, powder sample, dissolving method by ICP-MS) and troctolite (fine-grained plagioclase \pm olivine \pm pyroxene \pm silica glass assemblage, not spinel, and coarse-grained plagioclase xenolith, analyzed by LA-ICP-MS) of NWA 12279 is like the troctolite of Mg-suite. Still, not K, Th, U, and REEs (Figure 12). The coarse-grained plagioclase in NWA 12279 is an established xenolith from FANs. At the same time, the large-grained Mg-spinels originate in the crust-mantle boundary of the Moon, and the “olivine \pm pyroxene \pm silica glass” assemblage crystallizes during magmatic upwelling. Therefore, PST in NWA 12279 is an intrusive rock that crystallizes later than

FANs. At the same time, it shows that: (a) the NWA 12279 parent body was formed in the area outside the Procellarum KREEP Terrane (PKT) (Shervais & McGee, 1998) and (b) the partial melting of the lunar mantle does not necessarily require the participation of KREEP. The lunar mantle melt was formed by decompression melting (Prissel & Gross, 2020).

The assemblage of Mg-spinel phenocrysts and magmatic melt inclusions, troctolite, and anorthosite xenoliths in NWA 12279 show that the position of the early crystallized large granular spinels is located from the lower crust at depths >25 km. The crystallization isotherms of pyroxenes (Figure 9b), pyroxene crystallite and glass, silica glass, and the interstitial structure of troctolite indicate that the final crystallization depth of troctolite for NWA 12279 may be from less than 40 km (Lindsley & Andersen, 1983) to the surface of Moon.

5. Conclusions

All petrological, mineralogical, and geochemical evidence supports the following hypotheses: the Mg-rich parental melt was derived from the partial melting of lunar mantle material. The upwelling olivine-dominated cumulates from the mantle experience decompression melting to produce the Mg-rich primary melt. The magma-wall rock interactions bring the Mg-rich melt to the plagioclase-undersaturated anorthositic crust. These melts occurred as an immiscible liquid phase separation, which can be divided into an Mg-rich and a Si-rich phases. Liquid-phase immiscible separation may be an essential process of crust-mantle interaction in the early lunar evolution. Sizeable granular Mg-spinel phenocrysts are formed through assimilation and equilibrium crystallization at depths >25 km of the lower crust, where the residual melt carrying Mg-spinels and anorthosite xenoliths continues penetrating the anorthositic crust. As the temperature decreases, the fine-grained plagioclase first crystallizes. Then, the “olivines ± pyroxenes ± silica glass” assemblage crystallizes and forms an interstitial texture with the plagioclase at depths from <40 km to the surface of the Moon. The early crystallized spinels and FANs trapped by the melt are randomly distributed in the late-formed troctolite.

Our petrogenetic model of Mg-spinel-bearing lithologies is almost consistent with the petrogenesis of lunar troctolites by Prissel and Gross (2020), as their model suggests partial melting of the primary lunar mantle and intrusion of those melts into the anorthositic crust, followed by minor crustal assimilation in producing spinel-bearing lithologies. The widespread global distribution of spinel-bearing lithologies and Mg-suite suggests that the crust-mantle interaction is an essential magmatism process in the early evolution of the Moon. Liquid-phase immiscible separation, assimilation mixing, equilibrium crystallization, and fractional crystallization are essential forms of lunar crust-mantle interaction. In addition, NWA 12279, like the NWA 10401 Mg-suite lunar meteorite (Gross et al., 2020), shares all the characteristics of Mg-suite rocks from the Apollo collection, except that it is strongly depleted in REEs and incompatible elements. This observation indicates that NWA 12279 could represent an Mg-spinel-bearing Mg-suite rock from an area other than the PKT.

Conflict of Interest

The authors declare no conflicts of interest relevant to this study.

Data Availability Statement

All data associated with this article can be found in the manuscript, and the more detailed raw data are deposited in the Mendeley repository (Chen, 2023). The data on which this article is based are available in Dymek et al. (1975), Floss et al. (1998), Gross et al. (2014a, 2014b, 2020), Jackson et al. (2014), Lindstrom et al. (1989), Lindsley and Andersen. (1983), Mercer et al. (2013), Papike et al. (1996), Papike (1998), Prissel et al. (2014, 2016), Shearer et al. (2015), Shearer and Papike. (2005), Shervais and McGee. (1998, 1999), Warren. (1993), Wittmann et al. (2019), Xu et al. (2020), and references therein.

References

- Anders, E., & Grevesse, N. (1989). Abundances of the elements: Meteoritic and solar. *Geochimica et Cosmochimica Acta*, 53(1), 197–214. [https://doi.org/10.1016/0016-7037\(89\)90286-x](https://doi.org/10.1016/0016-7037(89)90286-x)
- Borg, L. E., Cassata, W. S., Wimpenny, J., Gaffney, A. M., & Shearer, C. K. (2020). The formation and evolution of the Moon's crust inferred from the Sm-Nd isotopic systematics of highlands rocks. *Geochimica et Cosmochimica Acta*, 290, 312–332.

Acknowledgments

This work is supported by the National Science Foundation of China (41866008) and Guangxi Scientific Base and Talent Special Projects, China (AD23026339 and AD23026084). The authors would like to express their gratitude to Edit-Springs (<https://www.editsprings.cn>) for the expert linguistic services provided and to the Guangxi Natural Museum of Earth Memory for the sample. Special thanks to the two reviewers Tabb C. Prissel and Allan Treiman, whose professional comments effectively improved the quality of the paper.

- Brown, R. W. (1977). A sample fusion technique for whole rock analysis with the electron microprobe. *Geochimica et Cosmochimica Acta*, 41(3), 435–438. [https://doi.org/10.1016/0016-7037\(77\)90273-3](https://doi.org/10.1016/0016-7037(77)90273-3)
- Chen, H. Y. (2023). The main and trace elements of NWA 12279 lunar meteorite [Dataset]. Mendeley Data, V1. <https://doi.org/10.17632/nhpdyrx89j.1>
- Dymek, R. F., Albee, A. L., & Chodos, A. A. (1975). Comparative petrology of lunar cumulate rocks of possible primary origin – Dunite 72415, troctolite 76535, norite 78235, and anorthosite 62237. In *Proc. Sixth lunar science conference* (Vol. 1, pp. 301–341).
- Elardo, S. M., Draper, D. S., & Shearer, C. K. (2011). Lunar Magma Ocean crystallization revisited: Bulk composition, early cumulate mineralogy, and the source regions of the highlands mg-suite. *Geochimica et Cosmochimica Acta*, 75(11), 3024–3045. <https://doi.org/10.1016/j.gca.2011.02.033>
- Elkins-Tanton, L. T., Van Orman, J. A., Bradford, H. H., & Grove, T. L. (2002). Re-examination of the lunar magma ocean cumulate overturn hypothesis: Melting or mixing required. *Earth and Planetary Science Letters*, 196(3–4), 239–249. [https://doi.org/10.1016/s0012-821x\(01\)00613-6](https://doi.org/10.1016/s0012-821x(01)00613-6)
- Floss, C., James, O. B., Mcgee, J. J., & Crozaz, G. (1998). Lunar ferroan anorthosite petrogenesis: Clues from trace element distributions in fan subgroups. *Geochimica et Cosmochimica Acta*, 62(7), 1255–1283. [https://doi.org/10.1016/s0016-7037\(98\)00031-3](https://doi.org/10.1016/s0016-7037(98)00031-3)
- Gross, J., Hilton, A., Prissel, T. C., Setera, J. B., Korotev, R. L., & Calzada-Diaz, A. (2020). Geochemistry and petrogenesis of northwest Africa 10401: A new type of the Mg-suite rocks. *Journal of Geophysical Research: Planets*, 125(5), e2019JE006225. <https://doi.org/10.1029/2019je006225>
- Gross, J., Isaacson, P. J., Treiman, A. H., Le, L., & Gorman, J. K. (2014). Spinel-rich lithologies in the lunar highland crust: Linking lunar samples with crystallization experiments and remote sensing. *American Mineralogist*, 99(10), 1849–1859. <https://doi.org/10.2138/am-2014-4780>
- Gross, J., & Treiman, A. H. (2011). Unique spinel-rich lithology in lunar meteorite ALHA 81005: Origin and possible connection to M³ observations of the farside highlands. *Journal of Geophysical Research*, 116(E10), E10009. <https://doi.org/10.1029/2011je003858>
- Gross, J., Treiman, A. H., & Mercer, C. N. (2014). Lunar feldspathic meteorites: Constraints on the geology of the lunar highlands, and the origin of the lunar crust. *Earth and Planetary Science Letters*, 388, 318–328. <https://doi.org/10.1016/j.epsl.2013.12.006>
- Herzberg, C. T., & Baker, M. B. (1980). The cordierite- to spinel-cataclasis transition: Structure of the lunar crust. In *Proc. conf. lunar highlands crust* (pp. 113–132).
- Hrstka, T., Gottlieb, P., Skála, R., Breiter, K., & Motl, D. (2018). Automated mineralogy and petrology—applications of TESCAN Integrated Mineral Analyzer (TIMA). *Journal of Geosciences*, 63(1), 47–63. <https://doi.org/10.3190/jgeosci.250>
- Jackson, C., Cheek, L. C., Williams, K. B., Hanna, K. D., Pieters, C. M., Parman, S. W., et al. (2014). Visible-infrared spectral properties of iron-bearing aluminated spinel under lunar-like redox conditions. *American Mineralogist*, 99(10), 1821–1833. <https://doi.org/10.2138/am-2014-4793>
- Lindsley, D. H., & Andersen, D. J. (1983). A two-pyroxene thermometer. *Journal of Geophysical Research*, 88(S02), A887–A906. <https://doi.org/10.1029/jb088is02p0a887>
- Lindstrom, M. M., Marvin, U. B., & Mittlefehldt, D. W. (1989). Apollo 15 Mg- and Fe-norites: A redefinition of the Mg-suite differentiation trend. In *Lunar and planetary science conference proceedings* (pp. 245–254).
- Liu, Y., Hu, Z., Gao, S., Günther, D., Xu, J., Gao, C., & Chen, H. (2008). In situ analysis of major and trace elements of anhydrous minerals by LA-ICP-MS without applying an internal standard. *Chemical Geology*, 257(1), 34–43. <https://doi.org/10.1016/j.chemgeo.2008.08.004>
- Marvin, U. B., Carey, J. W., & Lindstrom, M. M. (1989). Cordierite-spinel troctolite, a new Mg-rich lithology from the lunar Highlands. *Science*, 243(4893), 925–928. <https://doi.org/10.1126/science.243.4893.925>
- Mercer, C. N., Joy, K. H., & Treiman, A. H. (2013). New lunar meteorite northwest Africa 2996: A window into farside lithologies and petrogenesis. *Meteoritics & Planetary Sciences*, 48(2), 289–315. <https://doi.org/10.1111/maps.12056>
- Morgan, Z., Yan, L., & Hess, P. (2006). An experimental study of anorthosite dissolution in lunar picritic magmas: Implications for crustal assimilation processes. *Geochimica et Cosmochimica Acta*, 70(13), 3477–3491. <https://doi.org/10.1016/j.gca.2006.04.027>
- Papanastassiou, D. A., & Wasserburg, G. J. (1975). Rb–Sr study of a lunar dunite and evidence for early lunar differentiates. In *Proc. sixth lunar sci. conf.* (Vol. 2, pp. 1467–1489).
- Papike, J. J. (1998). Comparative planetary mineralogy: Chemistry of melt-derived pyroxene, feldspar, and olivine. *Reviews in Mineralogy and Geochemistry*, 36(2), G1–G11.
- Papike, J. J., Fowler, G. W., Shearer, K. C., & Layne, D. G. (1996). Ion microprobe investigation of plagioclase and orthopyroxene from lunar Mg-suite norites: Implications for calculating parental melt REE concentrations and for assessing postcrystallization REE redistribution. *Geochimica et Cosmochimica Acta*, 60(20), 3967–3978. [https://doi.org/10.1016/0016-7037\(96\)00212-8](https://doi.org/10.1016/0016-7037(96)00212-8)
- Pieters, C. M., Besse, S., Boardman, J., Buratti, B., Cheek, L., Clark, R. N., et al. (2011). Mg-spinel lithology: A new rock type on the lunar farside. *Journal of Geophysical Research*, 116(E6), 1–14. <https://doi.org/10.1029/2010je003727>
- Pieters, C. M., Kerri, D. H., Leah, C., Deepak, D., Tabb, P., Colin, J., et al. (2014). Taylor the distribution of Mg-spinel across the Moon and constraints on crustal origin. *American Mineralogist*, 99(10), 1893–1910. <https://doi.org/10.2138/am-2014-4776>
- Premo, W. R., & Tatsumoto, M. (1992). U–Pb Isotopes in dunites 72415. In *23rd lunar and planetary science conference* (pp. 1103–1104).
- Prinz, M., Dowty, E., Keil, K., & Bunch, T. E. (1973). Mineralogy, petrology and chemistry of lithic fragments from Luna 20 fines: Origin of the cumulate ant suite and its relationship to high-alumina and mare basalts. *Geochimica et Cosmochimica Acta*, 37(4), 979–1006. [https://doi.org/10.1016/0016-7037\(73\)90195-6](https://doi.org/10.1016/0016-7037(73)90195-6)
- Prissel, T. C., & Gross, J. (2020). On the petrogenesis of lunar troctolites: New insights into cumulate mantle overturn and mantle exposures in impact basins. *Earth and Planetary Science Letters*, 551, 116531. <https://doi.org/10.1016/j.epsl.2020.116531>
- Prissel, T. C., Parman, S. W., & Head, J. W. (2016). Formation of the lunar highlands Mg-suite as told by spinel. *American Mineralogist*, 101(7), 1624–1635. <https://doi.org/10.2138/am-2016-5581>
- Prissel, T. C., Parman, S. W., Jackson, C. R. M., Dhingra, D., Ganskow, G., Cheek, L., et al. (2012). Melt–wallrock reactions on the Moon: Experimental constraints on the formation of newly discovered Mg-spinel anorthosites. In *43rd lunar and planetary science conference* (p. 2743).
- Prissel, T. C., Parman, S. W., Jackson, C. R. M., Rutherford, M. J., Hess, P. C., Head, J. W., et al. (2014). Pink Moon: The petrogenesis of pink spinel anorthosites and implications concerning Mg-suite magmatism. *Earth and Planetary Science Letters*, 403, 144–156. <https://doi.org/10.1016/j.epsl.2014.06.027>
- Ryder, G. (1991). Lunar ferroan anorthosites and mare basalt sources: The mixed connection. *Geophysical Research Letters*, 18(11), 2065–2068. <https://doi.org/10.1029/91gl02535>
- Shearer, C. K., Elardo, S. M., Petro, N. E., Borg, L. E., & McCubbin, F. M. (2015). Origin of the lunar highlands Mg-suite: An integrated petrology, geochemistry, chronology, and remote sensing perspective. *American Mineralogist*, 100(1), 294–325. <https://doi.org/10.2138/am-2015-4817>
- Shearer, C. K., & Papike, J. J. (2005). Early crustal building processes on the Moon: Models for the petrogenesis of the Mg-suite. *Geochimica et Cosmochimica Acta*, 69(13), 3445–3461. <https://doi.org/10.1016/j.gca.2005.02.025>

- Shervais, J. W., & McGee, J. J. (1998). Ion and electron microprobe study of troctolites, norite, and anorthosites from Apollo 14: Evidence for urKREEP assimilation during petrogenesis of Apollo 14 Mg-suite rocks. *Geochimica et Cosmochimica Acta*, 62(17), 3009–3023. [https://doi.org/10.1016/s0016-7037\(98\)00195-1](https://doi.org/10.1016/s0016-7037(98)00195-1)
- Shervais, J. W., & McGee, J. J. (1999). Petrology of the western highland province: Ancient crust formation at the Apollo 14 site. *Journal of Geophysical Research*, 104(E3), 5891–5920. <https://doi.org/10.1029/1998je900025>
- Simon, S. B., Shearer, C. K., Haggerty, S. E., Moriarty, D. P., Petro, N., Papike, J. J., & Vaci, Z. (2022). Multiple shallow crustal origins for spinel-bearing lithologies on the Moon: A perspective from the Luna 20 mission. *Journal of Geophysical Research: Planets*, 127(11), e2022JE007249. <https://doi.org/10.1029/2022je007249>
- Smith, J. V., Anderson, A. T., Newton, R. C., Olsen, E. J., Crewe, A. V., Isaacson, M. S., & Wyllie, P. J. (1970). Petrologic history of the Moon inferred from petrography, mineralogy, and petrogenesis of Apollo 11 rocks. *Geochimica et Cosmochimica Acta*, 1, 897–925.
- Sun, Y., Li, L., & Zhang, Y. Z. (2017). Detection of Mg-spinel-bearing central peaks using M³ images: Implications for the petrogenesis of Mg-spinel. *Earth and Planetary Science Letters*, 465, 48–58. <https://doi.org/10.1016/j.epsl.2017.01.019>
- Treiman, A. H., Kulis, M. J., & Glazner, A. F. (2019). Spinel-anorthosites on the Moon: Impact melt origins suggested by enthalpy constraints. *American Mineralogist*, 104(3), 370–384. <https://doi.org/10.2138/am-2019-6652>
- Treiman, A. H., Maloy, A. K., Shearer, C. K., & Gross, J. (2010). Magnesian anorthositic granulites in lunar meteorites Allan Hills A81005 and Dhofar 309: Geochemistry and global significance. *Meteoritics & Planetary Sciences*, 45(2), 163–180. <https://doi.org/10.1111/j.1945-5100.2010.01014.x>
- Walker, D., & Hays, J. F. (1977). Plagioclase flotation and lunar crust formation. *Geology*, 5(7), 425–428. [https://doi.org/10.1130/0091-7613\(1977\)5<425:pfallcf>2.0.co;2](https://doi.org/10.1130/0091-7613(1977)5<425:pfallcf>2.0.co;2)
- Wang, K., Jacobsen, S. B., Sedaghatpour, F., Chen, H., & Korotev, R. L. (2015). The earliest Lunar Magma Ocean differentiation recorded in Fe isotopes. *Earth and Planetary Science Letters*, 430, 202–208. <https://doi.org/10.1016/j.epsl.2015.08.019>
- Warren, P. H. (1985). The Magma ocean concept and Lunar evolution. *Annual Review of Earth and Planetary Sciences*, 13(1), 201–240. <https://doi.org/10.1146/annurev.ea.13.050185.001221>
- Warren, P. H. (1986). Anorthosite assimilation and the origin of the Mg/Fe-related bimodality of pristine Moon rocks: Support for the magma-sphere hypothesis. *Journal of Geophysical Research*, 91(B4), D331–D343. <https://doi.org/10.1029/jb091ib04p0d331>
- Warren, P. H. (1993). A concise compilation of petrologic information on possibly pristine nonmare Moon rocks. *American Mineralogist*, 78, 360–376.
- Wittmann, A., Korotev, R. L., Jolliff, B. L., & Carpenter, P. K. (2019). Spinel assemblages in lunar meteorites Graves Nunataks 06157 and Dhofar 1528: Implications for impact melting and equilibration in the Moon's upper mantle. *Meteoritics & Planetary Sciences*, 54(2), 379–394. <https://doi.org/10.1111/maps.13217>
- Wood, J. A. (1972). Thermal history and early magmatism in the Moon. *Icarus*, 16(2), 229–240. [https://doi.org/10.1016/0019-1035\(72\)90070-x](https://doi.org/10.1016/0019-1035(72)90070-x)
- Xie, L. F., Chen, H. Y., Miao, B. K., Song, W. L., Xia, Z. P., Chen, G. Z., et al. (2023). A possible origin of the lunar spinel-bearing lithologies as told by the meteorite NWA 13191. *American Mineralogist*. <https://doi.org/10.2138/am-2022-8728>
- Xu, X. Q., Hui, H. J., Chen, W., Huang, S. C., Neal, C. R., & Xu, X. S. (2020). Formation of lunar highlands anorthosites. *Earth and Planetary Science Letters*, 536, 116238. <https://doi.org/10.1016/j.epsl.2020.116138>
- Yang, J., Ju, D. Y., Pang, R. L., Li, R., Liu, J. Z., & Du, W. (2023). Significance of silicate liquid immiscibility for the origin of young highly evolved lithic clasts in Chang'E-5 regolith. *Geochimica et Cosmochimica Acta*, 340, 189–205. <https://doi.org/10.1016/j.gca.2022.11.008>